11

FREQUENCY-INDEPENDENT ANTENNAS

We derive the idea of self-scaling or frequency-independent antennas from the principle of frequency scaling used in model measurements. As we decrease the wavelength (increase frequency), we decrease the model size in the same proportion. To build wideband antennas, we need structures that can be their own scale models. One approach is to remove any characteristic length by specifying the antenna only in terms of angles [1]. This method leads to the continuously scaled spiral antennas. A second approach is to include antenna parts that scale a portion of the antenna exactly at discrete frequency intervals. We scale these parts logarithmically so that the intervals between frequencies of perfect scaling grow with frequency. These log-periodically scaled antennas have varying characteristics between the points of scaling whose ripple decreases as the scaling constant approaches 1 (continuous scaling), but the number of parts increases.

A continuous or log-periodically scaled structure has no ends, but we must be able to truncate a successful frequency-independent antenna with little effect on the pattern. A self-scaling antenna must be a transmission-line structure that delivers power to an active region where we feed the high-frequency end, and it serves as a transmission line for the lower-frequency portion. The currents must decay after a radiating active region so that the structure can be stopped without adversely affecting antenna properties. We identify the finite active region by truncation constants that we use to size the design. Although the spiral radiates most of the input power in a finite active region, we improve the pattern by loading the ends of the arms to prevent radiation of currents flowing in the reverse direction and accept loss.

The active region radiates most of the power for a particular frequency. A true frequency-independent antenna has a constant beamwidth over its band, although we expect small variations between the frequencies of exact scalings (log periodic). We

Modern Antenna Design, Second Edition, By Thomas A. Milligan

obtain constant beamwidths only if the active-region dimensions scale with wavelength. The truncation requirement affects the pattern. A self-scaling antenna cannot radiate in the direction of the expanding structure. If the antenna did radiate in that direction, portions of the structure would be excited in higher-order modes beyond the normal truncation point. Log-periodic and conical logarithmic spirals backfire toward the feed point.

We can make a structure with logarithmically scaled radiating parts along a transmission line and still not achieve a successful broadband antenna. The parts must couple electromagnetically, not just through the connection of the feeder. We place dipoles of the log-periodic dipole antenna close together to produce the coupling needed for rapid attenuation. Similarly, we closely space the turns of a spiral so that the arms couple and there is sufficient length in the active region along which to radiate. Usually, we can account for the rapid attenuation of currents through loss of power in radiation by considering a single mode.

A successful self-scaling antenna structure satisfies these requirements [2]:

1. The antenna contains its own scale model parts—continuous or discrete—that can be scaled to an infinitesimal size.
2. The antenna radiates most of the power in a finite active region so that it can be terminated with minimal effect.
3. Fed from the high-frequency end, the antenna must be a transmission line to carry power to the low-frequency end.
4. The dimensions of the active region must scale with wavelength.
5. The antenna must not radiate in the direction of expanding structure.
6. The parts must have significant direct coupling outside the transmission-line feeder.

SPIRAL ANTENNAS

Spiral antennas consist of a thin metal foil spiral pattern etched on a substrate, usually fed from the center, and located over a cavity. The etching contains a symmetrical pattern of at least two arms, but we build spiral antennas with more arms to radiate in multiple modes or to suppress unwanted modes. The two-arm version can be fed using a simple balanced line requiring a balun. With more arms we need a feed network called a *beamformer*, which contains an output port for each spiral arm and a separate input for each spiral mode. This network ideally divides the power into equal-amplitude outputs with a linear phase progression between them. The phase progression of each spiral mode cycles one or more times through all phases, and the complex summation of any set of mode voltages equals zero. The number of complete rotations through all phases equals the mode number; mode 1 has one cycle, 2π radians; mode 2 has 2 cycles, 4π radians; and so on.

Figure 11-1 plots the measured pattern of an eight-arm equiangular spiral operating in mode 1 obtained from single-arm measurements added using an ideal feed network (beamformer). The pattern shows RHC polarization as co-polarization and LHC polarization as cross-polarization. This is the most commonly used mode. When we change the number of arms and feed them properly with mode 1, we obtain similar patterns.

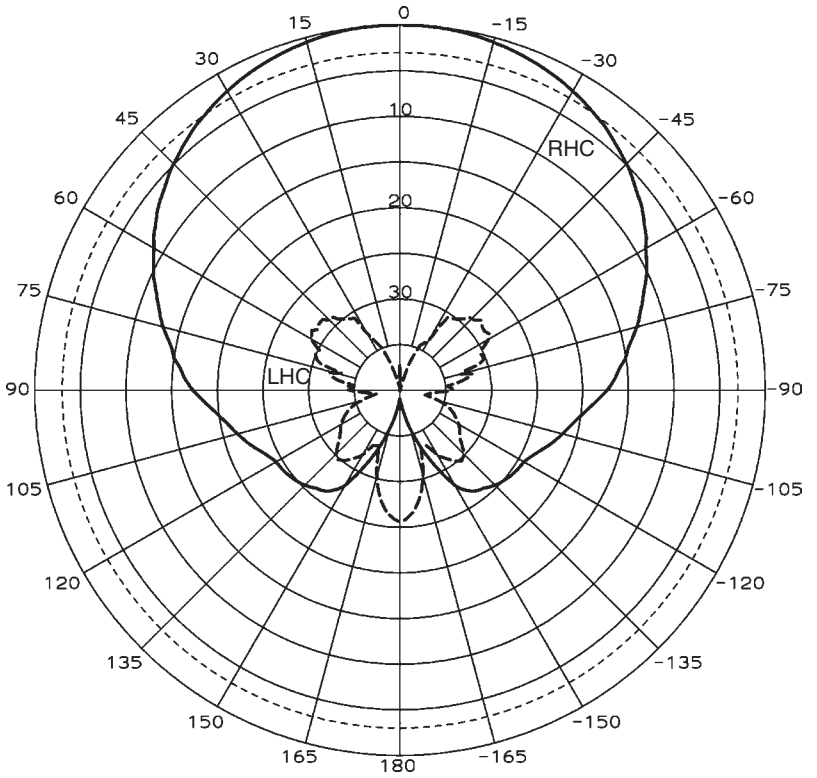

FIGURE 11-1 Measured pattern of an eight-arm spiral operating in mode 1 using an ideal beamformer.

The extra arms aid the pattern symmetry, because they suppress radiation of higher-order modes that distort the pattern. By building a spiral with more than two arms we can intentionally excite radiation of higher-order modes. Figure 11-2 gives the patterns of the eight-arm spiral radiating mode 2 when fed from an ideal beamformer. When we plot the pattern for mode 3, it is similar to the mode 2 except that the beam peak occurs at an angle farther from broadside. All higher-order modes of the spiral have a beam shape similar to mode 2 except that the beam peak angle continues to increase with mode number.

Each spiral mode radiation has a phase rotation of a full 2π radian cycles for conical patterns, which equals the mode number. A conical pattern measurement rotates ϕ about the spiral plane normal axis while holding θ constant. For example, we could measure patterns at $\theta = 45^\circ$ on the patterns of Figures 11-1 and 11-2 near the peaks of the higher-order modes. We determine the mode radiating by the phase slope. RHC polarization produces a negative slope as ϕ increases [counterclockwise (CCW) rotation]. We use the convention that positive modes radiate RHC and negative modes radiate LHC and place the negative sign in the mode expressions. Increasing the angle is similar to increasing the distance in terms of the radiation phase. By exciting the spiral in adjacent mode numbers, the phase difference between them can be used to determine the ϕ angle of arrival when one mode supplies the reference signal for phase measurement.

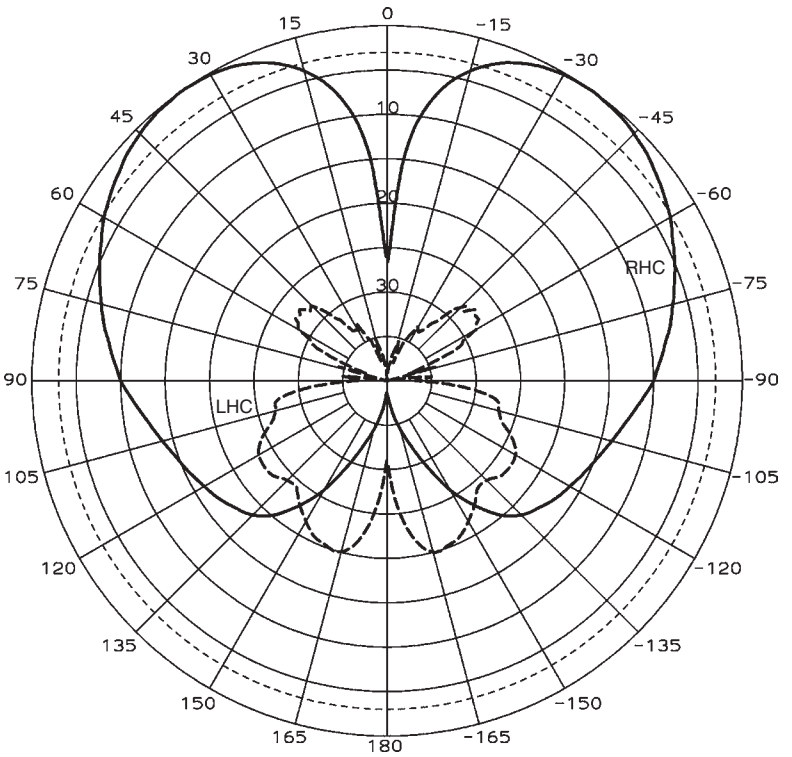

FIGURE 11-2 Measured pattern of an eight-arm spiral operating in mode 2 using an ideal beamformer.

We use multiple modes on the spiral for an angle of arrival (AOA) system by comparing two modes. The amplitude difference between modes 1 and 2 determines the angle off the axis of the spiral plane. Off-axis, where the higher-order modes radiate, we measure a phase progression equal to the mode; for example, mode 2 radiation changes by 720° as we rotate the antenna one revolution in a conic pattern. Given the mode number, the phase varies by $-m360^\circ$ during one revolution. If we use mode 1 as a phase reference, the phase of mode 2 relative to it changes -360° during one revolution about the spiral plane axis. By using both amplitude and phase, the two angles of arrival can be determined. Although a three-arm spiral will support both modes 1 and 2, necessary for AOA, we use a four-arm spiral because it uses a simpler feed network [3].

11-1 MODAL EXPANSION OF ANTENNA PATTERNS

We use a modal or Fourier series expansion of conical patterns for the analysis and measurement of spirals. A conical pattern varies ϕ while holding θ constant in the spherical coordinate system and is the AUT or head axis of a model tower positioner. Each term in the expansion includes the modal phasing of a circularly polarized signal. For example, the mode 1 phase has a single rotation -2π in the full CCW rotation of a conical pattern, mode 2 has a $-2(2\pi)$ phase rotation, and so on.

The mode number of a spiral refers to the number of 2π (radians) or 360° (degrees) cycles that occur in the feed phasing when progressing through the arms CCW. Mode 1 phases in a two-arm spiral are 0° and 180°. Cycling to the first input adds another 180°, to give 360° around the spiral arms. The phase difference moving CCW between arms is found from the mode number m and the number of arms N:

$$\text{phase} = -\frac{2\pi m}{N} \quad \text{or} \quad -\frac{360^\circ m}{N} \tag{11-1}$$

The spiral radiates RHC polarization for $m = 1$ using the notation of Eq. (11-1).

An axially symmetrical antenna such as a spiral can radiate these modes when we phase the feeding of the ports to match the phase rotation of the mode. We must add spiral arms to feed higher-order modes. Modes $+1$ and -1 produce the same phasing at the feed points of a two-arm spiral: 0° and 180°, and the spiral wrap direction determines the polarization radiated. All odd-order ($\ldots, -3, -1, 1, 3, 5, \ldots$) modes have the same phasing on two feeds, which means that the two-arm spiral will radiate these modes efficiently if current flows on the arms where the spiral circumference is the same integer number of wavelengths. The number of arms equals the number of independent modes, although the zero mode is difficult to use. You should expand Eq. (11-1) for various numbers of arms and modes. The sense of the spiral wrap and the direction of current flow determine the circular polarization sense. On an N-arm structure the modes have a cyclic variation, so that, for example, mode 3 of a four-arm spiral has phasing equivalent to $m = -1$ (i.e., mode 1 LHC polarization). In other words, the modes are modulo 4 with mode 3 equal mode -1. When feeding the right-hand four-arm spiral with mode 3 from the center, the spiral fails to radiate from the currents flowing out the arms because each arm radiates RHC while the feed phasing is LHC, and they cancel. The spiral acts as a circular polarization filter. These currents reflect from the ends of the open-circuited arms, travel inward, and radiate LHC polarization. On a two-arm spiral, whenever the circumference is an odd-integer multiple of a wavelength, the currents radiate. Increasing the number of arms to four from two reduces the number of modes radiating because modes 3, 7, and so on, phases no longer match the feeding phases of the arms. Only modes 5, 9, ... phases match mode 1.

When you apply Eq. (11-1) to an eight-arm spiral you will discover that for a rotation of five-cycles (mode 5) the phase shift between ports -225° equals the phasing of mode -3 135° and shows the modulo characteristic of modes. An eight-arm spiral has the following equivalences: mode -3 = mode 5, mode -2 = mode 6, mode -1 = mode 7. Although we can divide the feed voltages on an N-arm spiral into N orthogonal modes, the antenna can radiate any mode. For example, if we feed the center of a two-arm spiral in mode 1, it will radiate a large portion of the power when its circumference is 1λ. When the circumference is 2λ, the spiral would radiate mode 2 except that the 180° phase difference between the two arms cancels this radiation. The antenna radiates some power in mode 2 if the feed voltage balance and phasing is not perfect. Mode 3 radiates when the circumference is 3λ and radiates part of the remaining power on the two spiral arms because the feed phases on the arms do not cancel. If the spiral is large enough to have a circumference of 5λ, mode 5 will radiate from the two-arm spiral. Mode 4 radiation is canceled by the arm phasing. Given a spiral with N arms, the modes that have significant radiation are a multiple of the number of arms when fed with a perfect beamformer network [3]:

$$m_{\text{radiated}} = m + kN \qquad k = \ldots, -2, -1, 0, 1, 2, \ldots \tag{11-2}$$

N-arm spiral suppresses $N-1$ modes between possible modes given that the spiral circumference is large enough to support a particular mode. For example, a six-arm spiral excited in mode 1 will radiate modes 1, 7, 13, ..., −5, −11, ... and when excited in mode 2 it will radiate modes 2, 8, 14, ..., −4, −10, ..., and so on. If the antenna radiates sufficient power in the lower-order modes, little is left for the higher-order mode radiation and the patterns will be fine. Increasing the number of arms reduces the number of spiral modes radiated.

Given a conical pattern $F(\phi)$, we expand it in the Fourier series of modes and easily compute the expansion coefficients from an integral performed numerically on a measured pattern:

$$F(\phi) = \sum_{m=-\infty}^{m=\infty} E_m e^{-jm\phi} \qquad \text{where} \quad E_m = \frac{1}{2\pi}\int_0^{2\pi} F(\phi) e^{jm\phi}\, d\phi \tag{11-3}$$

Each conical pattern has its own set of modal coefficients $E_m(\theta)$ for each polarization. The polarizations are pairs of orthogonal polarizations, such as (E_θ, E_ϕ) or (E_{RHC}, E_{LHC}). We apply these modal coefficients when testing or analyzing spiral antennas as a measure of performance. We use an integral over the entire radiation sphere to determine the relative power in each mode:

$$P_m = \frac{\displaystyle\int_0^{\pi} \left[\left| \int_0^{2\pi} E_{\text{RHC}}(\theta,\phi) e^{jm\phi}\, d\phi \right|^2 + \left| \int_0^{2\pi} E_{\text{LHC}}(\theta,\phi) e^{jm\phi}\, d\phi \right|^2 \right] \sin\theta\, d\theta}{\displaystyle\int_0^{\pi}\int_0^{2\pi} [|E_{\text{RHC}}(\theta,\phi)|^2 + |E_{\text{LHC}}(\theta,\phi)|^2] \sin\theta\, d\phi\, d\theta} \tag{11-4}$$

Equation (11-4) is written in terms of the RHC and LHC polarizations, but we can substitute any other pair of orthogonal polarizations and use the same formula. The denominator is proportional to the total power radiated by the antenna.

11-2 ARCHIMEDEAN SPIRAL [4, 5]

Although Archimedean and exponential spirals have different equations defining them, practice shows that their characteristics do not differ by very much. The Archimedean spiral arm lengths can be long and produce high circuit losses at low frequencies. The wrap angle of an Archimedean spiral changes from a high value in the center to a low value on the outside. The high wrap rate in the center excites more higher-order modes at high frequencies. The low wrap rate at the outer diameter improves pattern shape at low frequencies. Although an exponential spiral has more uniform characteristics over the entire frequency range, an Archimedean spiral is useful.

The Archimedean spiral radius increases uniformly with angle:

$$r = r_0 + a\phi \tag{11-5}$$

where r_0 is the initial radius and a is the growth rate. We cannot scale the structure to an infinitesimal size by using Eq. (11-5), one of the requirements of frequency-independent antennas. Figure 11-3 shows two shapes of Archimedean spirals. We

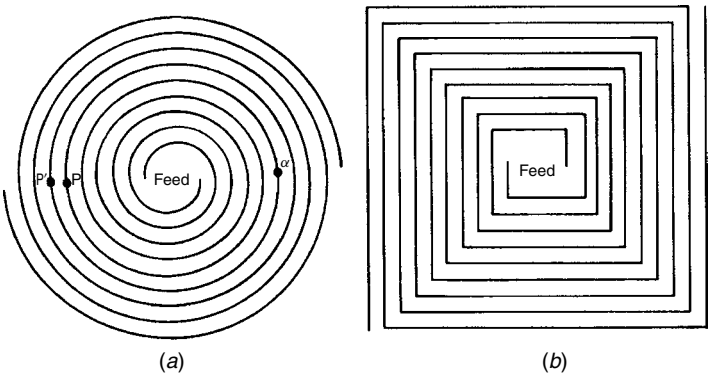

FIGURE 11-3 Archimedean spirals: (*a*) LHC; (*b*) RHC.

usually make the antenna complementary—the uniform-width metal strip equals the spacing between strips. A two-arm infinite structure has an impedance of 188 Ω from the Babinet–Booker principle (Section 5-3) for a self-complementary structure.

A balanced line feeds the spiral from the center. The radiations from the nearly equal and opposite currents at the feed point cancel in the far field. The growing spiral arms separate the currents. When the perimeter of the turn approaches one wavelength, the out-of-phase currents at P and Q (Figure 11-3) become in phase at points P and P', and radiation from the currents no longer cancel in the far field. This condition starts somewhat before the 1λ perimeter point and continues for some distance after it. To radiate efficiently the antenna should have a perimeter of 1.25λ at the lowest operating frequency. The upper-frequency truncation size is determined by a requirement to limit the spacing between feed points to less than $\lambda/4$, although to reduce radiation of higher-mode modes, they should be closer. For higher-mode operation, we increase the outer diameter to $(m + 0.25)\lambda/\pi$, and the spacing between the feed points can be increased to $m\lambda/4$.

A spiral radiates RHC polarization on one side and LHC polarization on the other side. We mount the antenna over a cavity to eliminate the unwanted polarization. The balun producing the balanced feed for a two-arm spiral can be mounted in the cavity. It converts the antenna from a coax input to prevent pattern squint and to limit higher-order mode radiation. Hand rules determine the sense of circular polarization. Let your fingers roll in the direction of the spiral (tips toward increasing radius) and the thumb points to the pattern maximum.

11-3 EQUIANGULAR SPIRAL

Rumsey [2] states that an antenna shape determined entirely by angles will be frequency independent because it is invariant to a change of scale. The biconical antenna satisfies the angle requirement but fails the truncation requirement for frequency independence because the current remains constant along its length and it fails the truncation requirement. An equiangular spiral antenna (Figure 11-4) defined by

$$r = r_0 e^{a\phi} \tag{11-6}$$

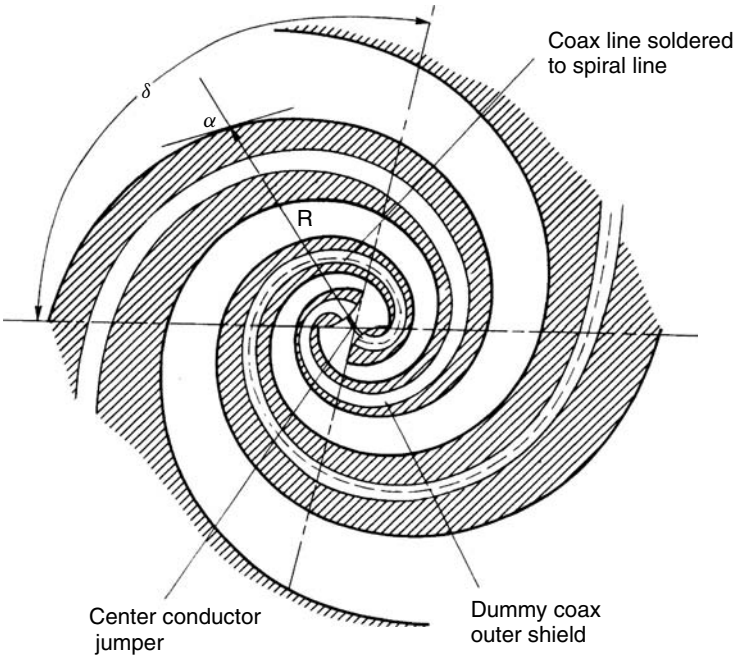

FIGURE 11-4 Equiangular spiral (RHC) with an infinite balun feeder.

is defined only by angles, since the inner radius can be related to an angle $r_0 = e^{a\phi_0}$ and satisfies the requirement for an antenna completely determined by angles. The wrap angle α (Figure 11-4) relates to the growth rate a of the spiral by

$$a = \frac{1}{\tan \alpha} \tag{11-7}$$

Another way of specifying the curves, the expansion factor (EF) specifies the ratio of radius increase in one turn; it is similar to the growth rate. The direct relationship to geometry makes it easy to specify:

$$a = \frac{\ln (\text{EF})}{2\pi} \quad \text{or} \quad \text{EF} = e^{2\pi a} \tag{11-8}$$

$$\text{EF} = \left(\frac{r_o}{r_i}\right)^{1/\text{turns}} \quad \text{or} \quad \text{Turns} = \frac{\ln (r_o/r_i)}{\ln (\text{EF})}$$

Angles also determine the width of the arms. We rotate the spiral by δ to generate the other edge of the spiral arm. We shift the angle ϕ by 180° (π) to generate the second arm. We also specify the spiral arms by the arm/gap ratio, so we can use noncomplementary arms as an impedance transformer. For δ specified in radians (substitute 360° for 2π if degrees) and N arms in the spiral, we can derive simple formulas between the two terms:

$$\delta = \frac{2\pi}{N\,(1 + \text{gap/arm})} \quad \text{or} \quad \frac{\text{gap}}{\text{arm}} = \frac{2\pi}{N\delta} - 1 \tag{11-9}$$

The input impedance of the antenna depends on the number of arms and the mode of operation. For complementary arms, or arm/gap = 1, an extension of the Babinet–Booker principle determines the impedance for a free-space spiral [6]:

$$Z_m = \frac{\eta_0/4}{\sin(\pi|m|/N)} \tag{11-10}$$

Equation (11-10) uses $\eta_0 = 376.73\ \Omega$ and positive m for the mode number where $m = 1, 2, \ldots, N-1$, whether RHC or LHC. Table 11-1 lists the characteristic impedance of N-arm multiterminal complementary structures in free space.

Table 11-1 does not give the impedance of a real spiral antenna because it will be mounted over a metallic cavity that will be either empty or partially filled with a multilayer sheet absorber. Second, the dielectric substrate on which the spiral is etched slows the waves on the arms and reduces the impedance by $1/\sqrt{\varepsilon_{r,\text{eff}}}$. Although these factors change the impedance, the table does illustrate the relative magnitudes of impedances for the various modes. We need to measure the spiral input impedance in its final configuration for its modes, which can be done using single-arm measurements of S_{11} and coupling to the other arms S_{21}. See Section 11-6 for this method.

We can impedance-match the antenna either for a single mode or for a compromise between modes by etching a tapered transformer at the spiral inputs. To vary the impedance we change the arm/gap ratio. The width of the spiral arms has only a minor effect on the pattern. An approach to this design uses the impedance of a coplanar strip transmission line for the complementary and noncomplementary structure to scale the impedances of the spiral [7]:

$$Z_{m,\text{noncomp}} = Z_{m,\text{comp}} \frac{Z_{\text{cp,noncomp}}}{Z_{\text{cp,comp}}} \tag{11-11}$$

Z_{cp} is the impedance of a coplanar stripline found from a model that includes multilayer substrates of lossy dielectrics, such as the absorber sheets [8, p. 70; 9]. The subscripts "noncomp" and "comp" refer to the noncomplementary and complementary line widths in the coplanar stripline and spiral. We generate a table by varying stripwidth/gap and calculate the impedance in the coplanar stripline and relate it to arm/gap of the spiral to determine equivalent impedance. This method starts with the impedance measurement

TABLE 11-1 Characteristic Impedance of N-Arm Multiterminal Complementary Structures in Free Space

Number of Arms	Mode 1	Mode 2	Mode 3	Mode 4	Mode 5	Mode 6	Mode 7
2	94.2						
3	108.8	108.8					
4	133.2	94.2	133.2				
5	160.2	99	99	160.2			
6	188.4	108.8	94.2	108.8	188.4		
7	217.1	120.5	96.6	96.6	120.5	217.1	
8	246.1	133.2	101.9	94.2	101.9	133.2	246.1

Source: [6].

for various modes of a complementary spiral in its final configuration. After generating a table relating arm/gap to spiral impedance, we design a tapered transformer using standard techniques and interpolating on the table for dimensions. When you vary the arm/gap ratio along the spiral arm, divide δ [Eq. (11-9)] into two parts ($\pm\delta/2$) and vary both sides of the strip centered on the central curve [Eq. (11-6)] so that the etched spiral pattern retains symmetry.

We integrate Eq. (11-6) to calculate arm length:

$$L = (r - r_0)\sqrt{1 + \tan^2 \alpha} = (r - r_0)\sqrt{1 + \frac{1}{a^2}} \tag{11-12}$$

We estimate the loss in the spiral by modeling the arm as a coplanar transmission line and calculating the transmission-line loss by including the finite conductive and dielectric loss tangent of the substrate and the nearest absorber layer in the cavity [8, p. 70]. Increasing the gap between the substrate and the first absorber layer reduces transmission-line loss. A few calculations using the multilayer model [9] will determine a suitable gap for the design. Feeding the spiral from the outside to radiate the opposite sense of circular polarization, a dual polarized design, can produce a design with long transmission-line lengths with high losses for the high frequencies whose active regions occur in the center of the spiral. Increasing the expansion factor will reduce the transmission-line losses of the spiral.

11-4 PATTERN ANALYSIS OF SPIRAL ANTENNAS

Measurement of spiral patterns shows that they do not have a null in the plane of the spiral, as predicted by a current sheet model, and that the antenna radiates cross-polarization in the upper hemisphere. A simple analysis model uses a traveling-wave loop in free space. This current distribution has constant amplitude on the loop, but its phase progresses linearly around the loop in integer cycles. Regardless of the actual circumference of the loop, a mode 1 current progresses through -360° (RHC) while mode 2 current phase changes -720° and, in general, mode m current rolls through $-m360^\circ$ for CCW movement along the loop. Mode 1 radiates from a loop 1λ in circumference and the general mode radiates from a loop $m\lambda$ in circumference when the current propagates with the free-space velocity. The loop size determines the pattern beamwidth and the effective loop size decreases when the spiral is dielectrically loaded by either the substrate or by dielectric slabs (lenses) and its beamwidth increases.

The traveling-wave loop model radiates only one mode because both the RHC and LHC signals have integer cycle phase progression in conic patterns. Modal expansion on the model patterns fails to indicate the level of cross-polarization of actual spirals when we use the ratio of integrals of the power in the co-polarized signal only to the sum of the power of both polarizations to determine cross-polarization loss. We need a better model for that characteristic and a way to predict higher mode radiation.

A method of moments (MOM) model of the spiral using a wire code such as NEC can predict the multiple-mode radiation of a spiral. The wire diameter in the model has little effect on the pattern predictions. Since it is difficult to model the absorber-loaded cavity in a MOM code, accurate impedance values cannot be obtained and fabricating antennas is the cost-effective method for finding impedance. You should

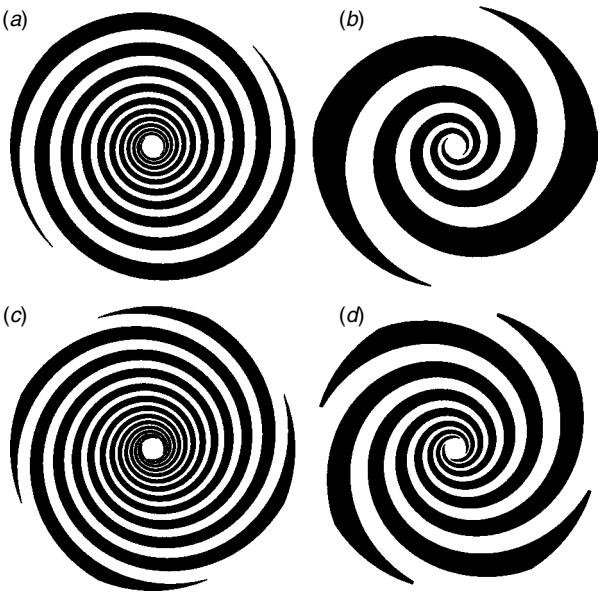

FIGURE 11-5 Equiangular spirals with differing expansion factors: (*a*) two-arm EF = 1.66; (*b*) two-arm EF = 3.32; (*c*) four-arm EF = 2.32; (*d*) four-arm EF = 4.64.

use the rotational symmetry capability of the code to reduce the model to a single-arm input so that the matrix is reduced by the number of arms N. We place the model in free space, which models the cavity as perfectly absorbing, and consider only the upper hemisphere.

Figure 11-5 illustrates the faces of two sets of two- and four-arm spirals designed to operate over a 10 : 1 frequency range. The inner diameter is 0.254λ. The left two-arm spiral contains five turns, with an expansion factor = 1.66 ($\alpha = 85.4^\circ$), while the looser-wrapped spiral on the right has 2.1 turns and EF = 3.32 ($\alpha = 79.15^\circ$). As we decrease the wrap angle (increased EF) the outer circumference of the spiral must be increased to support the lowest frequency. To illustrate the effect of the outer circumference, Table 11-2 lists the modal response of the five-turn (EF = 1.66) spiral versus outer circumference, and Table 11-3 lists the same results for the 2.1-turn (EF = 3.32) spiral. Scale 1-7 shows that the difference between mode 1 and mode -1 must be 9.6 dB to achieve a 6-dB axial ratio. The five-turn spiral needs an outer circumference of about 1.4λ at the lowest frequency for this value, while the 2.1-turn spiral should be 1.9λ. The looser-wrapped spiral requires a larger diameter to achieve the same

TABLE 11-2 Modal Response of a Two-Arm Exponential Spiral with *EF* = 1.66 ($\alpha = 85.4^\circ$), Five Turns

Circumference (λ)	Mode 1 (dB)	Mode -1 (dB)	Circumference (λ)	Mode 1 (dB)	Mode -1 (dB)
1.00	−1.96	−4.40	1.60	−0.16	−14.52
1.20	−1.09	−6.55	1.80	−0.05	−19.82
1.40	−0.46	−10.00	2.00	−0.04	−20.60

TABLE 11-3 Modal Response of a Two-Arm Exponential Spiral with $EF = 3.32$ ($\alpha = 79.16°$), 2.1 Turns

Circumference (λ)	Mode 1 (dB)	Mode −1 (dB)	Circumference (λ)	Mode 1 (dB)	Mode −1 (dB)
1.00	−2.34	−3.82	1.80	−0.53	−9.44
1.20	−1.81	−4.69	2.00	−0.34	−11.26
1.40	−1.25	−6.02	2.20	−0.21	−13.38
1.60	−0.82	−7.68	2.40	−0.12	−16.07

low-frequency axial ratio. These spirals have open-circuited arms. We reduce the axial ratio by loading the ends of the arms, which reduces the reflected mode radiation by the return loss of the loads relative to the spiral arm impedance. The efficiency decreases but the axial ratio improves.

An Archimedean spiral with 10.5 turns covers the same 10 : 1 frequency range. Table 11-4 gives the modal response. The tighter wrap of the spiral near the outer diameter reduces the diameter required to produce a lower axial ratio design. An outer circumference of 1.17λ is sufficient for a 6-dB axial ratio. The additional spiral arm length will reduce efficiency at the low-frequency end due to the transmission-line loss.

Increasing the number of turns will decrease the levels of the over-modes radiated. The two-arm spiral suppresses the even modes but allows radiation of modes 3, 5, 7, ... [Eq. (11-2)]. The moment method analysis predicts the over-mode levels given in Figure 11-6. The higher-order modes occur because the antenna is large enough to support these modes at higher frequencies but not at lower frequencies. Power not radiated in the mode 1 region near a 1λ circumference travels along the arms until it reaches the 3λ and 5λ circumferences and radiates. Over-modes alter conical patterns by adding amplitude and phase ripple. The phase ripple is added to the mode single 360° linear distribution. Mode 3 adds a single cycle ripple to conical patterns of mode 1, and mode 5 will add a two-cycle ripple on top of the single mode 3 cycle. At normalized frequency 9.5 for EF = 1.66, mode 3 at −10 dB relative to mode 1 produces an average peak-to-peak ripple of 5.7 dB (Scale 1-8) while the −23-dB mode 5 produces 1.2 dB of ripple. Amplitude and phase ripple is not a significant problem in most applications because we cannot use the antenna for an AOA system without two modes. Table 11-5 lists the mode 3 amplitude on the Archimedean spiral, which says that we must reduce the inner diameter to limit the over-mode level. For example, to limit it to −16.4 dB (2.6 dB of ripple), we need to reduce the inner diameter to 80% of 0.254λ (0.20λ). The Archimedean spiral requires a smaller feed diameter than the exponential spiral for the same over-mode level.

TABLE 11-4 Modal Response of a Two-Arm Archimedean Spiral with 10.5 Turns

Circumference (λ)	Mode 1 (dB)	Mode −1 (dB)	Circumference (λ)	Mode 1 (dB)	Mode −1 (dB)
1.00	−1.81	−4.68	1.20	−0.31	−11.68
1.05	−1.36	−5.70	1.25	−0.14	−14.92
1.10	−0.94	−7.13	1.30	−0.05	−19.34
1.15	−0.57	−9.11	1.35	−0.02	−24.04

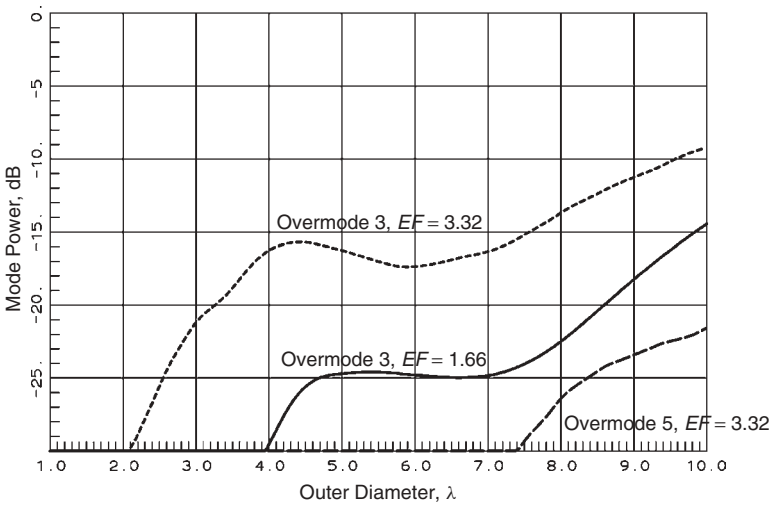

FIGURE 11-6 Over-modes of a two-arm spiral designed for a 10 : 1 frequency range.

TABLE 11-5 Mode 3 Relative Power for a 10 : 1 Archimedean Spiral with an 0.254λ Inner Diameter

Frequency	Power (dB)	Frequency	Power (dB)
7.2	−19.3	8.8	−14.0
7.6	−17.8	9.2	−13.0
8.0	−16.4	9.6	−12.0
8.4	−15.2	10.0	−11.0

The two examples of four-arm spirals exhibit results similar to those of two-arm spirals. Decreasing the expansion factor decreases high-order modes, and the phasing of the feed network eliminates additional modes. The four-arm spiral radiates mode 5 with a power of −13 dB relative to the total and the extra signal adds and subtracts with the mode 1 radiation to produce the four-way symmetry of the curves to the pattern deviation. The pattern ripple number equals the difference in mode number when two modes interact. The −13 dB extra radiation causes a 4-dB amplitude ripple (Scale 1-8) and 13° peak-to-peak phase variation (Scale 1-9). The similar levels of mode 6 shown in Figure 11-7 for mode 2 excitation produce pattern ripple. The AOA system uses the relative phase and amplitude between the two modes, and these extra signals cause the pattern variation to rotate in angular position as frequency changes. If we do not control the levels of the extra modes, AOA accuracy will suffer. In other applications the pattern fluctuation would be acceptable. Table 11-6 lists the modal response of a four-arm exponential spiral when fed for mode 2 and gives the size required to suppress mode −2 radiating cross-polarization.

To some extent we can feed the outer arms to radiate the opposite-sense circular polarization. The signals reach the circumference of higher-mode radiation before reaching the circumference of lower-order radiation. The spiral radiates substantial power in the higher-order modes which reduces the signal traveling inward to the

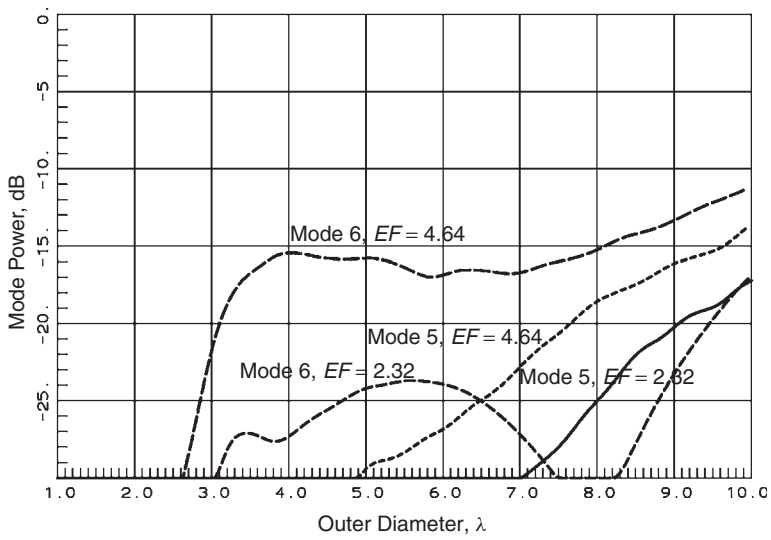

FIGURE 11-7 Over-modes of a four-arm spiral designed for a 10 : 1 frequency range.

TABLE 11-6 Modal Response of a Four-Arm Exponential Spiral with $EF = 2.07$ ($\alpha = 83.4^\circ$), 3.5 Turns Fed for Mode 2

Circumference (λ)	Mode 2 (dB)	Mode −2 (dB)	Circumference (λ)	Mode 2 (dB)	Mode −2 (dB)
2.00	−1.91	−4.49	2.80	−0.25	−12.6
2.20	−1.33	−5.78	3.00	−0.13	−15.4
2.40	−0.82	−7.64	3.20	−0.07	−18.1
2.60	−0.46	−10.0	3.40	−0.04	−20.3

lower-order-mode radiation circumference. We increase the number of arms to suppress the higher-mode radiation through phase cancellation produced by the feed network. Figure 11-8 shows the radiation levels of mode −1 for different number of arms. The outer circumference is 1λ at the lowest frequency for mode −1. We see an initial efficiency loss for the two-arm spiral in mode −1. Higher order modes have more restricted frequency regions.

Locating the spiral wire above a ground plane models a reflective cavity antenna to some extent, but it does not include the effects of the cylinder walls. The reflection of the waves from the ground plane will excite higher-mode currents farther out in the spiral, which increases the modal content of the pattern and limits the usable frequency band of the antenna. For example, a two-arm spiral fed for mode 1 with an initial depth of λ/8 has a mode 3 level at −8 dB when the cavity depth is λ/2. When the cavity depth is λ/2, the mode 1 pattern has a null at broadside. To produce an antenna with a wider bandwidth, we need a shallower cavity. The closer ground plane increases the power reflected into higher modes and the over-modes problem increases. We reduce the over-modes by increasing the number of arms to cancel modes through the feeding phases.

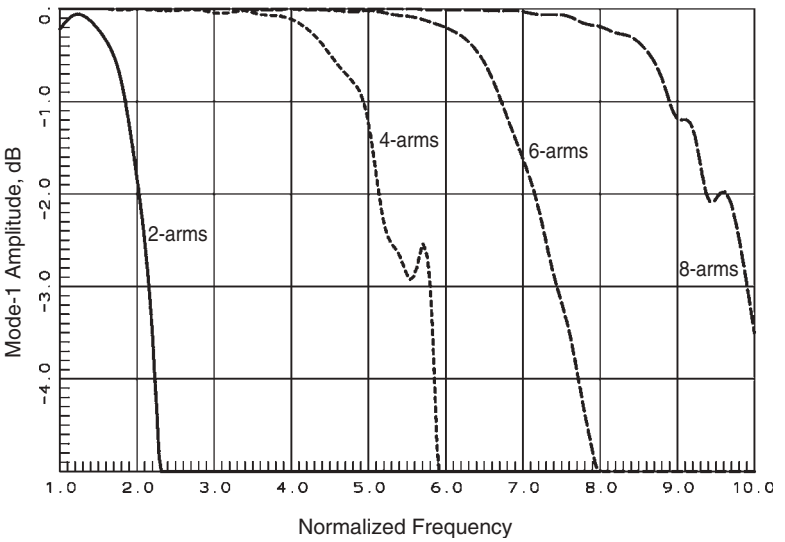

FIGURE 11-8 Efficiency of outside arm feeding of spirals designed for a 10 : 1 frequency range for mode −1 for different numbers of arms.

11-5 SPIRAL CONSTRUCTION AND FEEDING

11-5.1 Spiral Construction

We etch the spiral pattern on a thin dielectric sheet. We should specify a circuit board with a low-loss tangent because the spiral operates as a transmission line between the arms whose length becomes significant for tightly wrapped spirals. This transmission can be analyzed as a coplanar strip transmission line for losses, and the equivalent dielectric constant of the transmission line loads the spiral and reduces the effective loop radiator size. We can further load the antenna by placing dielectric sheets above the spiral or by placing a contact lens on the spiral face and shrink the spiral diameter.

Although it is not necessary to place a resistive load on the end of the spiral arms, it will improve the polarization at low frequencies by reducing reflections that radiate the opposite sense of circular polarization. Reflected currents travel inward and pass through the radiation regions of the spiral. Spirals fed from both inside and outside contain transmission-line feeds that load each arm; otherwise, we use a resistive paste or film on the last turn, but the antenna may produce acceptable patterns without loads on the arms.

We can use a reflective cavity under the spiral to prevent radiation of the opposite sense of circular polarization, but it limits the bandwidth. Waves reflected from the cavity base couple back into the spiral arms beyond the lower-mode radiation region. These waves excite spiral currents that travel to the next radiation region or into the loads on the ends. Without these loads the currents would reflect and travel inward to radiate in the first active region of an oppositely sensed circularly polarized mode.

We load the base of the cavity with absorber to build a wideband antenna. A tapered or stepped loaded absorber prevents reflection over a wideband. You should space the absorber away from the spiral face so that it does not significantly load the transmission line of the spiral arms. We analyze this absorber loading as an element in a coplanar

strip transmission line containing multiple lossy dielectric layers. A foam or dielectric honeycomb spacer between the absorber and the spiral circuit board prevents thermal or mechanical stress movement that severs the board connections.

Simple analysis says that half the power will be radiated into the absorber and reduce the gain by 3 dB. Unfortunately, the wave impedance of the absorber loaded cavity is much less than the impedance of free space. In an admittance model of the radiation in free space and the cavity, the power divides between the shunt loads of the two regions and the lower cavity impedance causes more than half of the power to be dissipated in the cavity, which further reduces the gain. We can recover some of this lost power by loading the spiral with a hemispherical contact lens that lowers the effective radiation impedance in the two-shunt-load model. The hemispherical lens has little effect on pattern shape since the outer surface does not refract rays that pass through normal to it. A lens with a dielectric constant in the range 2 to 3 increases gain by 1.5 to 2 dB, but it reduces the efficiency of mode radiation in the active region and leads to increased cross-polarization and over-mode levels.

A contact lens can decrease the beamwidth of a spiral besides decreasing the cavity absorber loss. Applying the technique of Section 9-4 and solving for a lens surface, we obtain the lens in Figure 11-9*a*, which shows the traced ray refraction for $\varepsilon_r = 2.55$. The lens surface can only refract rays straight upward out to an angle of 51°, but the side cylinder continues to refract rays from the feed upward. Figure 11-9*b* and *c* shows the measured pattern for a four-arm spiral operating in modes 1 and 2 with a 1.25λ-diameter contact lens on it. The lens reduced the beamwidth of mode 1 from 70° to 32° and mode 2 from 42° to 25° when we compare these patterns with Figures 11-1 and 11-2. The mode 2 beam peak moved from 35° to 22°. The lens design uses a point source, but the spiral radiates from rings approximately 0.33λ (mode 1) and 0.66λ (mode 2) in diameter. Nevertheless, the lens produces remarkable results with a mode 2 ring current one-half its diameter. The lens continued to shrink the beamwidths in a linear function as frequency increased. Similar results were reported using a hemispherical lens raised above the spiral [3]. This example demonstrates that small lenses have a significant effect on antenna patterns, whereas a reflector of this size would be useless.

11-5.2 Balun Feed

We feed a two-arm spiral with a balanced line, whereas spirals with more arms require a beamformer network. A balanced line feeder contains equal and oppositely phased currents when fed from a balun. The two common baluns used for spirals are the Marchand balun, a compensated sleeve balun (Section 5-15.2), and Bawer and Wolfe [11] version of the Roberts balun (Section 5-15.1), a compensated folded balun. We place the Marchand balun below the cavity to position its balance wire output in the center and we feed a two-wire line across the cavity to feed the spiral. We locate the two sleeves of the Marchand balun parallel to the cavity base. The Bawer and Wolfe balun is constructed on two sides of a printed circuit board oriented along the vertical axis. The balanced output is a short distance from the feed point and we feed two wires through to the etched board of the spiral. The printed circuit board causes a small asymmetry in the cavity and the absorber must be removed around the board so that it does not load it. Because mode 1 impedance is greater than 50 Ω, we can use a tapered microstrip balun similar to the split-tube coaxial balun to feed the two-arm spiral.

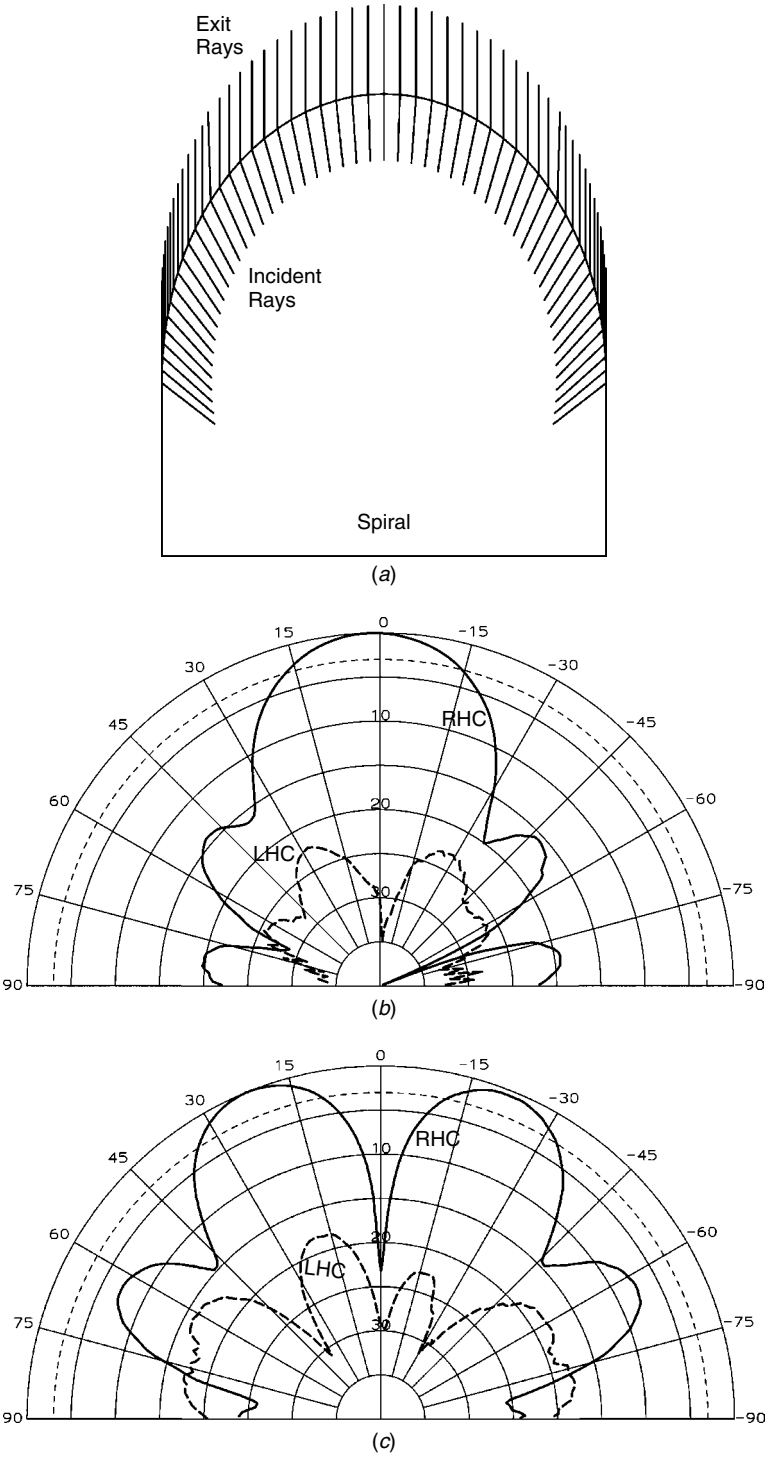

FIGURE 11-9 Measured patterns of a 1.25λ-diameter contact lens mounted over a spiral: (*a*) ray trace in polyethylene lens; (*b*) mode 1 pattern; (*c*) mode 2 pattern.

11-5.3 Infinite Balun

We can make a balun by using the truncation property of the spiral where the current attenuates rapidly beyond the active region. The balun prevents currents excited on the outside of a coax from reaching the input. In Figure 11-4 we solder the coax feeder to one of the arms. Since the antenna does not radiate in the direction of the expanding arms, it does not excite currents on the structure after the active region; conversely, no currents excited on the structure beyond the active region will reach the input. The coax feeder outer shield becomes part of the antenna. We solder a dummy coax on the second arm to maintain symmetry.

Because the balun uses the active region limitation on currents of the antenna, its bandwidth matches that of the antenna. We use the same balun structure for log-periodic dipole antennas when similar truncation requirements can be used to form the balun. This construction requires wide spiral traces for soldering, a difficult operation to perform over the long arm length. To shorten the arm length, we use spirals with low wrap angles, but they have poor radiation characteristics.

11-5.4 Beamformer and Coaxial Line Feed

Spirals with more than two arms require the direct feeding of each arm with a coaxial line. We feed phase-matched cables through the cavity and connect them to a microwave circuit that generates modal excitations. The beamformer provides a separate input port for each mode desired. The coax center conductors feed the spiral arms while we join the outer conductors. The spiral mode currents sum to zero, which means that the currents on the outer conductors also sum to zero. When feeding the inside, we strap the outer conductors together by using a ribbon connected to all shields or route the cables through a metal cylinder. The cylinder stops short of the spiral circuit board but is connected to the cavity bottom. For perfect modal feeding the current in the cylinder is zero. When we feed the outer arms of the spiral, we etch a shorting disk on the opposite side of the spiral face. We connect each coaxial cable outer conductor to this ring. By connecting the shorting disk to the outer wall of the cavity, we produce another path for the currents to sum to zero.

The design and construction of beamformers is beyond our discussion. We use a Butler matrix as a beamformer for spirals with 2^N arms (2, 4, 8, etc.), which provides a separate input port for the complete set of modes, while beamformers for spirals with 3, 5, 6, etc. arms present a challenge. Complete analysis of the spiral involves measurements of the spiral arms and the beamformer.

11-6 SPIRAL AND BEAMFORMER MEASUREMENTS [12]

We measure antenna patterns of the assembly of the spiral and the beamformer and determine the modal content by applying Eq. (11-4). Of course, we extract the normal pattern parameters of gain, beamwidth, beam direction, cross-polarization, and possibly phase center from the measurements. The final antenna can radiate in many modes, whereas the beamformer N_{arm} outputs can operate only in N_{arm} modes. During construction we gain insight and can correct problems by making single-arm measurements of the spiral and single port measurements of the beamformer.

The beamformer outputs can be expanded in N_{arm} modes, where each mode has equal amplitude on the outputs and a different phase progression in cycles of 2π radians. The feeding coefficients on arm N, for mode m, are given by

$$V_N = \frac{\exp[-j2\pi m(N-1)/N_{\text{arm}}]}{\sqrt{N_{\text{arm}}}} \tag{11-13}$$

where we number the arms CCW when looking at the spiral face. We calculate the modal expansion levels by multiplying network analyzer measurements of the arm responses b_n by the complex conjugate of Eq. (11-13) and adding over the arms. This is a summation version of Eq. (11-4) used for antenna patterns:

$$b_m = \sum_n V^*_{n,m} b_n \tag{11-14}$$

We repeat these measurements for each spiral mode of the beamformer and expand them in modes given by Eq. (11-14) to detect beamformer construction problems.

We measure the antenna pattern for each spiral arm separately while placing resistive loads on the other ports. This is the scan (active) pattern of each arm in a co-located array. The close arm spacing generates high mutual coupling that excites currents on all arms even though only one arm is fed. Measurement using an automated pattern system allows digital storage of all patterns that can be added using the measured outputs of the beamformer or an ideal beamformer to determine the final pattern. We apply Eq. (11-4) to the combined single-arm measurements to calculate the mode levels radiated for each input mode. Except for a ϕ rotation, all single-arm measurements should be the same. We gain insight into the construction of each arm by duplicating a single-arm measurement to produce N_{arm} copies and rotating $N_{\text{arm}} - 1$ of them, applying an ideal or measured beamformer responses, and calculating the resulting pattern to determine modal content. Construction differences between the arms become readily apparent. Of course, we may reduce the initial measurement effort during development by measuring a single arm and assuming ideal construction between arms. The other arms must be present so that the single arm couples to them and excites currents on them.

***S*-Parameter and Impedance Measurements** We use a network analyzer to measure the coupling to the other arms as well as the input reflection of each arm. We compute the input impedance for each mode by combining the reflection coefficient of a single arm with the others loaded (S-parameter) and the mutual coupling to the other arms weighted by the mode voltages [Eq. (11-13)]. Our analysis of the multiarm spiral as an array allows the use of the scan impedance. If we assume construction symmetry initially, we measure with only one arm as input. We load the outputs of the spiral arms if this is the final configuration; otherwise, we leave them with open-circuited terminations. The resulting reflection coefficient is found from

$$\Gamma_1 = \frac{b_1}{a_1} = S_{11} + S_{12}\frac{a_2}{a_1} + S_{13}\frac{a_3}{a_1} + \cdots + S_{1N}\frac{a_N}{a_1} \tag{11-15}$$

The coefficients a_i are the arm modal coefficients whose sum of magnitude squared equals 1, and S_{ij} are the mutual coupling values.

For spirals with arms loaded on the ends, we replace the loads with connectors and measure the coupling from the inputs to the loads. The power dissipated in each load depends on the mode. We denote the arm output ports as $N_{\text{arm}} + 1$ to $2N_{\text{arm}}$ in CCW order and measure the output wave on each arm:

$$\begin{aligned} b_{N+1} &= S_{N+1,1}a_1 + S_{N+1,2}a_2 + S_{N+1,3}a_3 + \cdots + S_{N+1,N}a_N \\ b_{N+2} &= S_{N+2,1}a_1 + S_{N+2,2}a_2 + S_{N+2,3}a_3 + \cdots + S_{N+2,N}a_N \\ &\vdots \\ b_{2N} &= S_{2N,1}a_1 + S_{2N,2}a_2 + S_{2N,3}a_3 + \cdots + S_{2N,N}a_N \end{aligned} \tag{11-16}$$

We sum the magnitude squared of b_{N+1} to b_{2N} to calculate the power dissipated in the loads [Eq. (11-16)] after we apply the modal coefficients a_i for a given mode. Equation (11-15) calculates the reflected power $1 - |\Gamma|^2$ and Eq. (11-16) determine the power dissipated in loads. We separate the antenna input power into the terms: (1) reflected, (2) dissipated in loads, (3) radiation, (4) circuit losses, and (5) power absorbed in the cavity. The power absorbed in the cavity and the circuit losses are only mildly frequency dependent. The sum of the first two terms will indicate the frequency range where the antenna has correct dimensions for efficient radiation and we can determine truncation constants with these bench measurements.

11-7 FEED NETWORK AND ANTENNA INTERACTION [8, pp. 347–353; 13]

The analysis above assumes an ideal feed network with perfect isolation between the output ports and impedance-matched ports on the antenna, the spiral arms, but the real feed network has limited isolation and the antenna ports are often mismatched. We encounter the same problem when dealing with a phased array because the input impedance of each element changes when we scan the beam. We use the subdomain growth method to solve these problems. The antenna has N ports matched by the same number of outputs on the feed network. We measure the $N \times N$ mutual coupling matrix of the antenna S_{RR} and the complete S-parameter matrix between the outputs of the feed network S_{QQ}, also $N \times N$. The normal connection matrix between the input and the feed network outputs S_{PQ} is $1 \times N$; the analysis in Section 11-6 used this matrix. We measure the input reflection coefficient S_{pp}, a single-element matrix, and then combine the matrices into an overall $(2N + 1) \times (2N + 1)$ matrix:

$$\begin{bmatrix} b_P \\ b_Q \\ b_R \end{bmatrix} = \begin{bmatrix} S_{PP} & S_{PQ} & [0] \\ S_{PQ}^{\mathrm{T}} & S_{QQ} & [0] \\ [0] & [0] & S_{RR} \end{bmatrix} \begin{bmatrix} a_P \\ a_Q \\ a_R \end{bmatrix} \tag{11-17}$$

The term [0] is an $N \times N$ null matrix.

We form a $2N \times 2N$ connection matrix between the antenna ports R and the feed network output ports Q using an $N \times N$ identity matrix $[I]$:

$$\begin{bmatrix} -S_{QQ} & [I] \\ [I] & S_{RR} \end{bmatrix}$$

We invert this matrix by partitioning it and obtain the matrix

$$\begin{bmatrix} S_{RR}(I - S_{QQ}S_{RR})^{-1} & (I - S_{RR}S_{QQ})^{-1} \\ (I - S_{QQ}S_{RR})^{-1} & S_{QQ}(I - S_{RR}S_{QQ})^{-1} \end{bmatrix} = \begin{bmatrix} M_{11} & M_{12} \\ M_{21} & M_{22} \end{bmatrix} \tag{11-18}$$

Since we have no direct inputs to the antenna elements, the analysis reduces to

$$[a_Q] = M_{11}S_{QP}a_P \quad \text{and} \quad [a_R] = M_{21}S_{QP}a_P \quad \text{with} \quad [a_Q] = [b_R] \tag{11-19}$$

The element a_P is the input to the feed network, and $[a_R]$ and $[a_Q]$ are the inputs to the antenna ports and the feed network output ports. We compute the input voltage vector to the antenna elements as $[V] = [a_R] + [b_R] = [a_R] + [a_Q]$. The input power to the elements is $P = [a_R]^{\mathrm{T}}[a_R]^* - [a_Q]^{\mathrm{T}}[a_Q]^*$ and the input reflection is $b_P = S_{PP} + S_{PQ}[a_Q]$. With this method we determine the effects of a non-perfect-feed network on the spiral or phased-array patterns when we use these excitations to calculate the pattern.

11-8 MODULATED ARM WIDTH SPIRAL [3, 14]

We have limited ability to feed a spiral from the outside for radiation of the opposite sense of circular polarization, LHC, from a right-hand wound spiral because we need many arms to suppress undesirable radiation (Figure 11-8) over a significant bandwidth. Modes -2 and -3 have a more restrictive bandwidth because the current reaches a higher-mode radiation point before the inner circumference of a particular mode and radiates. The modulated arm width (MAW) spiral solves these problems. We feed this antenna from the center to obtain the negative modes assuming that the spiral is wound right-hand. If we feed a right-hand spiral with left-hand modes, the current flows through the spiral with little radiation and in a normal spiral current reflects from the open-circuited arm ends and travels inward. Traveling backward on the spiral, the currents radiate LHC polarization at integer multiples of a wavelength circumference not suppressed by the phasing of multiple arms. Unfortunately, the complete trip of the current through the spiral to the ends of the arms and back to the radiation circumference adds to the transmission-line loss of the antenna.

Figure 11-10 shows the construction of this antenna for four, six, and eight-arms. We modulate the arm width to form a bandstop choke (filter) that reflects currents whose center wavelength increases at the same rate as the spiral diameter. The number of modulation cycles around one spiral turn equals the number of arms. For analysis we consider the spiral as a transmission line in the nonradiating regions whose arm/gap ratio determines the characteristic impedance. When the length of the modulation section approaches $\lambda/4$, the impedance mismatch at one discontinuity adds with the next one, and the numerous reflections build to form a bandstop choke response that increases with the line-width ratio. When the distances between the steps are substantially less than $\lambda/4$, the reflections fail to add coherently and cancel.

A four-arm MAW spiral has eight steps around one turn that locates a high reflection point at a 2λ circumference. If we feed the center of a four-arm spiral with mode 3, which equals mode -1 (LHC), the current travels outward on a right-hand-wound spiral with little radiation. The current reflects where the spiral circumference is 2λ

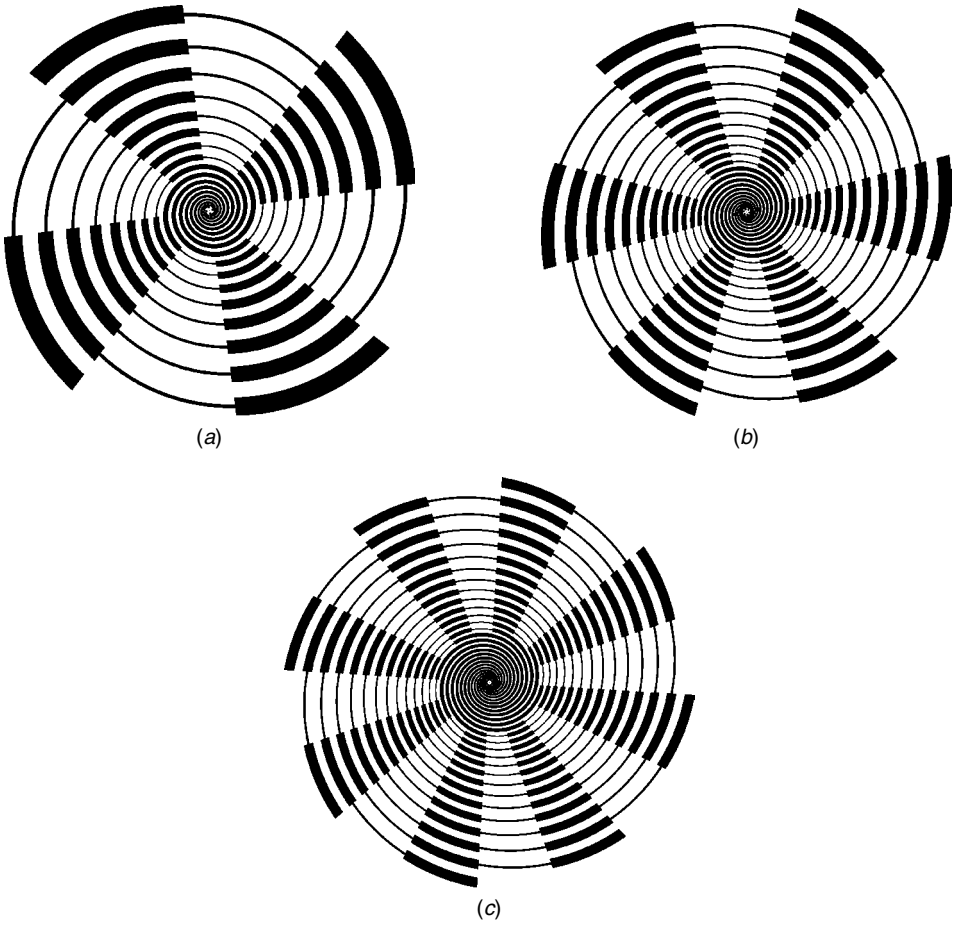

FIGURE 11-10 Modulated arm spirals: (*a*) four-arm; (*b*) six-arm; (*c*) eight-arm.

due to the bandstop chokes before it reaches the 3λ circumference and counterrotates to the 1λ circumference, where it radiates LHC polarization in mode −1. On the other hand, mode 1 radiates from the currents before they reach the bandstop region at a 2λ circumference, and the modulations have little effect. Of course, residual power left on the spiral after the first radiation region causes pattern ripple that varies over frequency, but the bandstop choke reduces radiation of mode 2 from the four-arm MAW spiral because the current reflects in the middle of the 2λ radiation region.

In a similar manner, a six-arm MAW spiral reflects the current at 3λ circumference and eight-arm MAW spiral at 4λ. The six-arm spiral with its reflection point at 3λ circumference can support modes −1 (5) and −2 (4). Both the six-arm feed phasing and the 3λ circumference bandstop choke suppresses mode −3 radiation when we feed it with mode −1 (5). The MAW spiral radiates mode 2 at a 2λ circumference before the current reaches the bandstop filter region at 3λ. Whereas a normal six-arm spiral can radiate mode 3, the MAW spiral cuts off its radiation because the bandstop region occurs at a 3λ circumference located at the middle of its active region. At this circumference both mode 3 and mode −3 exist and radiate to produce a linearly

polarized wave. In a similar manner the eight-arm spiral with its 4λ circumference bandstop filter can support modes 1, 2, 3, −1 (7), −2 (6), and (−3) 5. The eight-arm feeding suppresses mode −3 radiation [Eq. (11-2)] when fed mode 7 (−1), although the currents pass through the 3λ circumference point.

It would seem that we must construct a larger antenna to support the radiation of these reflected modes. The four-arm spiral effectively radiates only modes 1 and −1, and the bandstop region occurs at a circumference of 2λ. At the low-frequency end of the band, we can use the reflection from the open circuits on the ends of the arms instead of the bandstop filter. It is unnecessary to start modulating the arm width in the spiral center until approaching the bandstop filter region of the highest frequency. This eases construction problems and allows normal connection in the center to the many arms. We can also use this center section to construct a tapered transformer for impedance matching by varying the arm/gap ratio.

11-9 CONICAL LOG SPIRAL ANTENNA [15, 16]

When we form the equiangular spiral on a cone, the antenna radiates predominantly toward the vertex and we gain some control of the beamwidth. The antenna projected on a cone continues to satisfy the truncation condition: Radiation is reduced along the structure. We modify the beamwidth by varying both the cone angle θ_0 and the wrap angle δ (Figure 11-11). The antenna is a slow-wave structure from the feed on

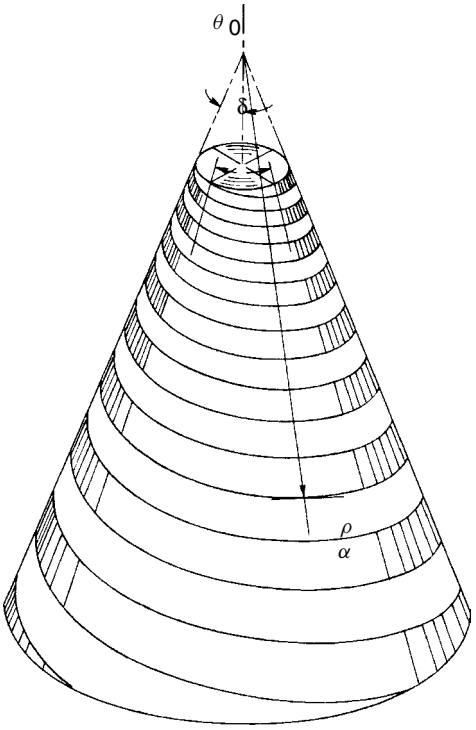

FIGURE 11-11 Two-arm conical log spiral antenna (RHC).

the upper diameter to the active region, but in the active region the antenna changes to a fast-wave structure to radiate a backfire pattern toward the cone vertex. Because the spiral on the cone radiates a unidirectional pattern, it reduces the radiation of one circular polarization sense. The flat spiral radiates equally on both sides, but because the pattern has a null in the direction of increasing structure, we can bend it downward on the cone and decrease the radiation of one sense of circular polarization. Figure 11-12 shows the calculated pattern of a conical spiral and illustrates the reduced back lobe and reduced cross-polarization caused by the conical shape.

We describe the spiral arms by the radius from the cone apex:

$$\rho = \rho_0 e^{b\phi} \qquad \text{where} \quad b = \frac{\sin\theta_0}{\tan\alpha} \tag{11-20}$$

We measure the angle of the spiral α with respect to the radius ρ along the cone. The angle δ determines the stripwidth, since Eq. (11-20) describes every edge of the spiral within an offset angle of ϕ. The length of the spiral strip edge is

$$L = (\rho - \rho_0)\sqrt{1 + \frac{1}{b^2}} = (\rho - \rho_0)\sqrt{1 + \frac{\tan^2\alpha}{\sin^2\theta_0}} \tag{11-21}$$

As θ_0 approaches $\pi/2$ (90°), we have the flat equiangular spiral.

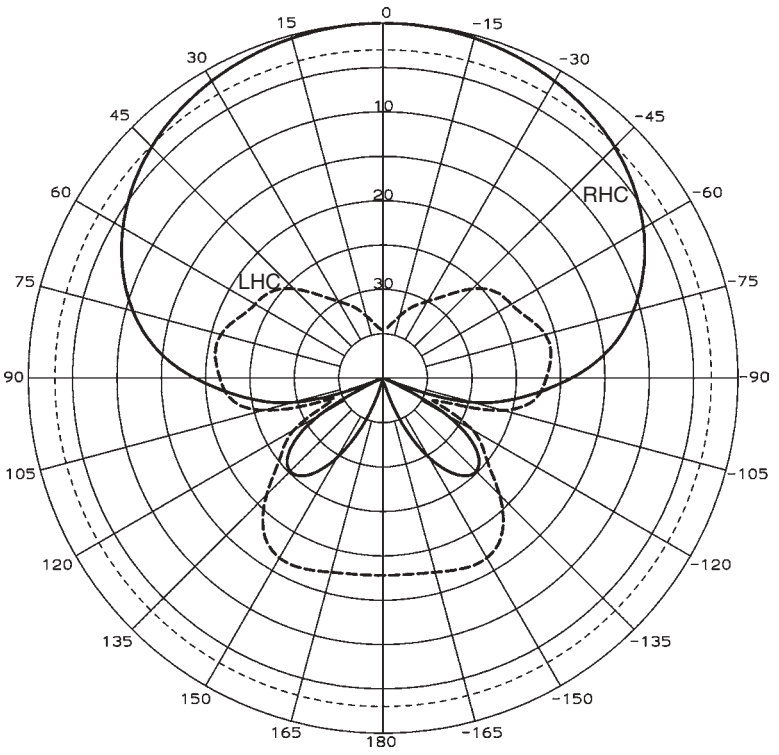

FIGURE 11-12 Calculated pattern of a two-arm conical spiral with a 30° total cone angle, $\alpha = 80°$, 11 turns.

We can describe the conical spiral using an expansion factor. Equation for the radius from the axis r is the same as the radius from the virtual apex ρ:

$$r = \rho_0 \sin\theta_0 e^{b\phi} = r_0 e^{b\phi}$$

In terms of the expansion factor, we have

$$b = \frac{\sin\theta_0}{\tan\alpha} = \frac{\ln(\text{EF})}{2\pi} \text{ or } \text{EF} = \exp\left(\frac{2\pi\sin\theta_0}{\tan\alpha}\right)$$

We rearrange these equations to compute the wrap angle α and the number of turns:

$$\alpha = \tan^{-1}\frac{2\pi\sin\theta_0}{\ln(\text{EF})} \quad \text{and} \quad \text{turns} = \frac{\tan\alpha\ln(r_o/r_i)}{2\pi\sin\theta_0}$$

Dyson [16] measured a large number of antennas to determine their properties, and we reduce his results to design tables. Table 11-7 gives the average beamwidth of the conical spiral. If we increase the wrap angle (tighter spiral) or decrease the cone angle (longer antenna), the beamwidth decreases and directivity increases. As we decrease the wrap angle to increase the beamwidth, the variation in beamwidth of various pattern cuts through the cone vertex increases because there are too few turns to maintain pattern symmetry, due to over-modes caused by an inefficient active region.

We specify the active region by upper and lower cone diameters. Dyson found a correlation between the band edges and the level of near-field probed currents. The current peaks in the active region, and in terms of design we can remove those portions of the antenna where the current drops by 3 dB on the high-frequency (small) end and 15 dB on the lower-frequency (large) end without affecting performance. These near-field current points give us upper and lower truncation diameters to scale the design. If we allow small changes in the beamwidth at the low-frequency end, we can use the 10-dB point to determine the lower diameter from the lowest operating frequency and make a smaller antenna. Tables 11-8 and 11-9 list the radiuses of the circles truncating

TABLE 11-7 Average Half-Power Beamwidth of a Two-Arm Conical Log Spiral Antenna ($\delta = 90°$)

Wrap Angle, α (deg)	Twice Cone Angle					
	$2\theta_0 = 2°$	$2\theta_0 = 5°$	$2\theta_0 = 10°$	$2\theta_0 = 15°$	$2\theta_0 = 20°$	$2\theta_0 = 30°$
90	36	49	55	60	65	70
85	37	50	58	64	68	74
80	38	53	63	70	74	81
75	41	56	70	78	83	90
70	44	60	79	88	95	103
65	47	65	89	100	108	119
60	52	71	102	114	127	139
55	57	79	115	132		
50	63	89				
45	69	106				

TABLE 11-8 Two-Arm Conical Log Spiral Antenna Upper Radius of Active Region (a_3^-/λ), Where the Current Drops 3 dB from the Peak

Wrap Angle, α (deg)	Twice Cone Angle						
	$2\theta_0 = 2^\circ$	$2\theta_0 = 5^\circ$	$2\theta_0 = 10^\circ$	$2\theta_0 = 15^\circ$	$2\theta_0 = 20^\circ$	$2\theta_0 = 30^\circ$	$2\theta_0 = 45^\circ$
85	0.119	0.111	0.106			0.091	
80	0.101	0.096	0.090	0.084	0.080	0.071	0.067
75	0.089	0.084	0.078	0.074	0.069	0.067	
70	0.078	0.074	0.069	0.066	0.060	0.057	
65	0.071	0.067	0.062	0.058	0.052	0.053	
60	0.063	0.059	0.054	0.050	0.045	0.046	
55	0.057	0.053	0.049	0.043	0.039		
50	0.052	0.048	0.043	0.035	0.036		
45	0.046	0.043		0.031	0.032		

TABLE 11-9 Two-Arm Conical Log Spiral Antenna Lower Radius (a_{10}^+/λ) of Active Region (Slightly Degraded Pattern), Where the Current Drops 10 dB from the Peak

Wrap Angle, α (deg)	Twice Cone Angle					
	$2\theta_0 = 2^\circ$	$2\theta_0 = 5^\circ$	$2\theta_0 = 10^\circ$	$2\theta_0 = 15^\circ$	$2\theta_0 = 20^\circ$	$2\theta_0 = 30^\circ$
85	0.136	0.144	0.150			0.174
80	0.117	0.128	0.132	0.147	0.156	0.164
75	0.106	0.120	0.132	0.144	0.156	0.172
70	0.100	0.118	0.130	0.144	0.159	0.185
65	0.096	0.117	0.131	0.145	0.168	0.215
60	0.095	0.116	0.132	0.150	0.178	0.250
55	0.095	0.116	0.134	0.156	0.186	
50	0.096	0.116		0.166	0.200	
45	0.098	0.117		0.180	0.215	

the cone at the end of the active region as functions of wrap angle and cone angle to be used to scale a design.

Example Design a conical log spiral with cone angle of 10° and wrap angle of 75° from 1 to 3 GHz.

$2\theta_0 = 20^\circ$. From Table 11-8, the upper truncation constant $a_3^-/\lambda = 0.069$. From Table 11-9, the lower truncation constant $a_{10}^+/\lambda = 0.156$. We use the radius a_3^-/λ with 3 GHz to determine the upper cone diameter and the radius a_{10}^+/λ with 1 GHz to determine the lower cone diameter:

$$\text{upper diameter} = 1.38\,\text{cm} \qquad \text{lower diameter} = 9.36\,\text{cm}$$

We compute the cone height from the projected central trapezoid:

$$\text{height} = \frac{D_L - D_u}{2\tan\theta_0} = 22.63\,\text{cm}$$

TABLE 11-10 Average Front/Back Ratio (dB) for a Conical Spiral Designed for the 10 : 1 Frequency Range Given the Cone Angle and Winding Wrap Angle

Cone Angle, 2θ	Wrap Angle (deg)								
	60	62.5	65	67.5	70	72.5	75	77.5	80
20	13.5	15.7	17.7	19.6	21.5	23.0	24.5	26.3	28.7
30	6.1	6.6	7.0	10.1	10.2	11.6	13.1	15.0	17.1
40					5.3	6.5	7.8	9.1	10.5

We determine the sense of circular polarization from the projection of the spiral on a plane ($\theta_0 = 90^\circ$) and by using hand rules with radiation toward the vertex. We use the same mode theory as the flat spiral to describe the radiation modes. The two-arm conical spiral radiates from the mode 1 with its peak on the boresight (on the axis). Table 11-10 lists the average front-to-back ratios for conical spirals averaged over a 10 : 1 frequency range and shows that long, thin cones produce the best F/B values.

Paraboloid Reflector Feed We can use the conical log spiral antenna as a broad bandwidth circularly polarized feed for a paraboloid reflector. The phase center moves along the cone axis when the frequency changes, but the illumination loss due to phase error is minor. Analysis of a number of possible feeds shows that the phase-center location depends almost entirely on cone geometry, not on wrap angle. The optimum location is dependent on the reflector f/D to a minor extent, but the location given by Table 11-11 is close to the optimum. Flatter cones have the phase center near the 1λ circumference, and as we narrow the cone it moves toward the virtual apex. Figure 11-12 for the conical spiral has a wider beamwidth than the flat spiral of Figure 11-1 because the phase center of the conical spiral occurs at 0.88λ circumference, whereas the spiral active region is centered at 1λ. The active region of this conical spiral has little axial length, which does decrease the beamwidth of the long, thin antennas (Table 11-7).

Table 11-12 lists the parameters of three conical spirals operating in mode 1 that produce the lowest average illumination losses as a paraboloid feed for designs that cover a 10 : 1 frequency range. Each design uses a wrap angle of 80° to reduce the pattern variation over the frequency range and to increase the F/B ratio to reduce spillover loss. Except for the lowest frequency range, the antennas have nearly constant beamwidth and produce nearly constant spillover and amplitude taper losses. Table 11-13 illustrates that varying reflector f/D has a slowly changing effect on the total average losses.

TABLE 11-11 Phase-Center Location of a Mode 1 Conical Spiral Relative to the Virtual Apex

Cone Angle, $2\theta_0$ (deg)	Axial Distance from Virtual Apex (λ)	Circumference (λ)
20	0.746	0.826
30	0.522	0.880
40	0.408	0.933

TABLE 11-12 Optimum Conical Spiral Mode 1 Feeds for a Paraboloid Reflector for a 10 : 1 Frequency Range

Cone Angle, $2\theta_0$ (deg)	f/D	Phase Error Loss (dB)		Taper Loss (dB)	Spillover Loss (dB)	Cross-Polarization Loss (dB)	Average Total (dB)
		Average	Maximum				
20	0.46	0.36	1.00	0.43	0.54	0.09	1.42
30	0.42	0.22	0.60	0.42	0.63	0.16	1.45
40	0.38	0.19	0.55	0.50	0.60	0.28	1.56

TABLE 11-13 Effect of Reflector f/D on Total Average Illumination Losses of the Designs of Table 11-12 (dB)

Cone Angle, $2\theta_0$ (deg)	Reflector f/D								
	0.34	0.36	0.38	0.40	0.42	0.44	0.46	0.48	0.50
20	2.24	1.97	1.76	1.61	1.51	1.44	1.42	1.42	1.44
30	1.68	1.55	1.48	1.45	1.45	1.47	1.53	1.60	1.68
40	1.63	1.58	1.56	1.58	1.63	1.70	1.79	1.89	2.00

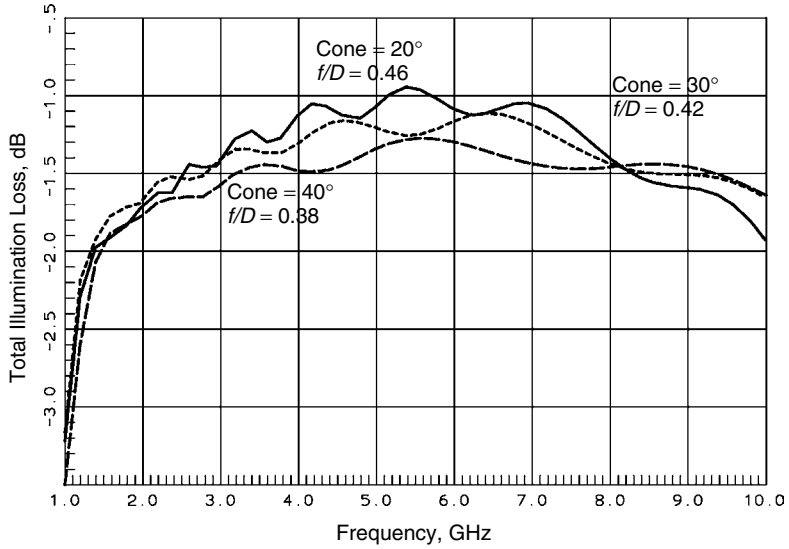

FIGURE 11-13 Total illumination losses for two-arm spirals designed for 1 to 10 GHz using Tables 11-8 and 11-9 feeding a paraboloid reflector.

Figure 11-13 gives the frequency response of the three reflector feeds. The narrower 20° design produces better reflector illumination over a narrower frequency range than that for the wider cones because the antennas were designed using truncation constants from Table 11-9, where the fields drop by 10 dB instead of 15 dB and the low-frequency pattern degrades.

11-10 MODE 2 CONICAL LOG SPIRAL ANTENNA

Conical log spiral antennas have limited available design information [17,18,19]. The beams off the boresight have half-power beamwidths ranging from 48 to 60°. Higher wrap angles and smaller cone angles decrease the beamwidth, but within this limited range. We cannot increase the axial length of the active region beyond a certain point, which limits the achievable gain. Although we have limited control of beamwidth, we can control the beam direction by the wrap angle. Table 11-14 lists the approximate beam peak given wrap angle on a 10° cone log spiral. Antennas built with cone angles in the range $2\theta_0 = 20$ to 40° follow Table 11-14 closely.

We must increase the diameters of the bottom and top of the four-arm mode 2 spiral from those calculated for the two-arm mode 1 conical log spiral. We obtain a suitable lower truncation constant from Dyson's results (Tables 11-8 and 11-9) if we multiply the lower truncation diameter by 1.42. The upper truncation constant multiplier varies linearly from 4 at $\alpha = 65°$ to 2.3 at $\alpha = 80°$. Since a little extra length on the top of the antenna will not degrade the pattern or increase the height significantly, we use the lower value for all designs.

Example Design a four-arm mode 2 conical log spiral antenna to point the beam at 50° over the frequency range 500 to 1500 MHz on a 10° cone.

Table 11-14 determines the wrap angle to scan the beam to 50°, $\alpha = 67°$. Table 11-8 gives us the upper truncation radius of the two-arm mode 1 spiral (0.055). Multiply by 2.3 for the mode 2 spiral:

$$\frac{a_3^-}{\lambda} = 2.3(0.055) = 0.126 \qquad \text{mode 2}$$

Similarly, Table 11-9 gives us the 10-dB lower truncation radius (0.165). We multiply it by 1.42 to calculate the lower truncation radius of the mode 2 spiral:

$$\frac{a_{10}^+}{\lambda} = 1.42(0.165) = 0.234 \qquad \text{mode 2}$$

We use a_3^-/λ with the highest frequency (1500 MHz) to determine the upper radius and use a_{10}^+/λ with the lowest frequency (500 MHz) to determine the lower radius of

TABLE 11-14 Beam Direction of a Mode 2 Conical Log Spiral Antenna for $2\theta_0 = 20°$

Wrap Angle, α (deg)	Beam Peak, θ (deg)	Wrap Angle, α (deg)	Beam Peak, θ (deg)
38	82	62	58
42	80	66	52
46	76	70	46
50	74	74	41
54	70	78	38
58	64		

Source: [19].

the truncated cone of the antenna:

$$D_U = 5.04\,\text{cm} \qquad D_L = 28.08\,\text{cm}$$
$$\text{height} = \frac{D_L - D_U}{2\tan\theta_0} = 65.33\,\text{cm}$$

11-11 FEEDING CONICAL LOG SPIRALS

We must feed the two-arm mode 1 spiral with a balanced line. The infinite balun consisting of coax soldered to the windings uses the truncation properties of the antenna to prevent currents induced on the outside of the coax from reaching the input. On the top we connect the center conductor of the coax to the second winding, which contains a dummy coax, to maintain symmetry. The coax length and associated loss become prohibitive for many spirals. We shorten the coax length by using a split tapered coax balun along the cone axis. Its bandwidth matches the antenna bandwidth.

It is difficult to tell if the four-arm mode 2 conical spiral antenna needs a balun. The pattern null on axis reduces the induced currents on the outside of a coax and we achieve suitable patterns without a balun. In some cases we see narrowband pattern distortion caused by the interaction of the outer-shield currents and higher-order modes. These cause pattern ripple in roll plane patterns (constant θ) near the beam peak. We can feed the antenna from four coax lines along the axis. We feed each winding separately and obtain cancellation of currents among the four shields soldered together.

Dyson says that we obtain the best patterns from complementary antennas—spacing equal stripwidth. The Babinet–Booker principle (Section 5-3) predicts an impedance of 188 Ω for a flat two-arm complementary spiral and 94 Ω for the four-arm spiral. Forming the spiral on a cone lowers the input impedance to about 150 Ω for the two-arm spiral and 85 Ω for the four-arm spiral. We can vary the stripwidth in the same way as a flat spiral to impedance-match the antenna with minor effects on the pattern.

LOG-PERIODIC ANTENNAS

All continuously scaled antennas radiate circular polarization. The point of constant beamwidth rotates with frequency. We can build linearly polarized self-scaling antennas only with structures that scale at discrete frequency intervals. The pattern characteristics will ripple between exact scaling frequencies, but with closely spaced scalings the antenna is practically frequency independent.

Every log-periodic structure has a basic scaling cell where we scale every dimension throughout the antenna by a constant:

$$\frac{f_1}{f_2} = \frac{\lambda_2}{\lambda_1} = \tau \qquad \text{scaling constant} \quad \tau < 1$$

The antenna will scale exactly at the sequence of frequencies: $f_n = f_0/\tau^n$. We make the antenna periodic in the logarithm of frequency with every dimension scaled by τ from element to element.

Log-periodic antennas were developed in the late 1950s out of modifications to the conical spiral concept of an antenna specified by angles. We will depart from an historical development and discuss the log-periodic dipole antenna first.

11-12 LOG-PERIODIC DIPOLE ANTENNA [20–23]

The design of a log-periodic antenna proceeds in two parts. First, the desired pattern characteristics determine the required number of elements in the active region and the element spacing. Second, we determine truncation points from the current levels on the antenna to establish the number of elements required for a given frequency range. As is true of the conical spiral, only a limited range of gains is possible because the aperture length is limited.

Figure 11-14 shows the log-periodic dipole antenna with a crisscross feeder line. We denote the longest dipole length by L_1. The element ends lie along lines that meet at the virtual apex. We measure the distance from the virtual apex to the dipole by R_n. The distance between elements is d_n. Starting with initial dimensions L_1, R_1, and d_1, we iterate all other dimensions by using the scaling constant τ:

$$L_2 = \tau L_1 \qquad R_2 = \tau R_1 \qquad d_2 = \tau d_1 \qquad L_3 = \tau L_2 = \tau^2 L_1 \qquad \text{etc.}$$

In general,

$$L_n = \tau^{n-1} L_1 \qquad R_n = \tau^{n-1} R_1 \qquad d_n = \tau^{n-1} d_1 \tag{11-22}$$

Note: d_n is not an independent variable, since

$$d_n = R_n - R_{n+1} = R_n(1 - \tau) \tag{11-23}$$

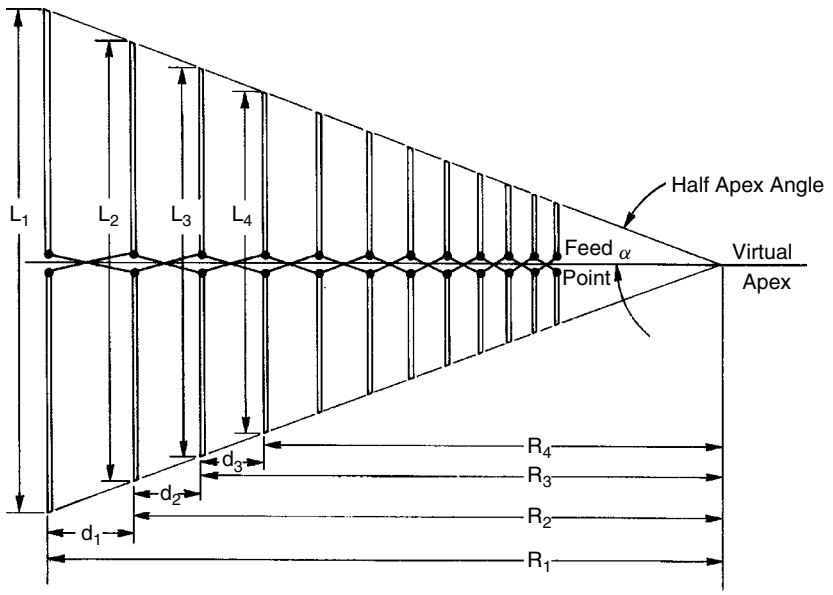

FIGURE 11-14 Log-periodic dipole antenna.

The angle between the dipole endpoints and the centerline—α, the half apex angle—is given by

$$\alpha = \tan^{-1} \frac{L_n}{2R_n} \tag{11-24}$$

Carrel introduced a spacing constant σ as a second constant to describe the antenna:

$$\sigma = \frac{d_n}{2L_n} \tag{11-25}$$

We specify the log-periodic dipole antenna by the constants τ and σ. We can compute α, the half apex angle, from τ and σ:

$$\alpha = \tan^{-1} \frac{1 - \tau}{4\sigma} \tag{11-26}$$

A method of moment analysis combining coupling between dipoles and transmission-line networks (Section 10-3.1) [23] was used to calculate the frequency response of a number of designs. These results were averaged over the operating frequency to obtain the values in tables below. Log-periodic dipole responses contain narrow-frequency-range regions where the pattern becomes distorted and the analysis summaries disregarded these regions. Nevertheless, the antenna response varies significantly. Table 11-15 lists the average gain for length/element diameter as 70. The element diameters were scaled by τ to maintain the same ratio (L/d) throughout the antenna. Tables 11-16 and 11-17 list the E- and H-plane average beamwidths over a suitable range of parameters τ and σ. The beamwidths vary between scaled frequency points. We use Tables 11-15 to 11-17 to determine suitable design constants. Although these tables give the average values for gain and beamwidth, the values have considerable ripple about the average that increases as τ is reduced.

We combine the desired operating frequency range with upper and lower truncation constants determined for τ and σ to compute the length of the longest element and

TABLE 11-15 Calculated Average Gain of a Log-Periodic Dipole Antenna for Length/Diameter = 70

	Scaling Constant, τ								
σ	0.80	0.82	0.84	0.86	0.88	0.90	0.92	0.94	0.96
0.06	6.0	6.5	6.0	6.0	6.9	7.2	7.9	8.6	9.7
0.07	5.2	6.1	6.9	6.8	6.9	7.6	8.2	9.0	10.1
0.08	5.5	5.6	6.7	7.2	7.1	7.8	8.4	9.2	10.4
0.09	6.0	5.7	6.0	7.3	7.7	7.8	8.8	9.6	10.7
0.10	6.6	6.4	6.1	6.5	7.7	8.2	8.8	9.7	10.9
0.12	6.5	6.9	7.3	7.5	7.7	8.3	9.3	10.1	11.4
0.14	6.3	6.7	7.1	7.5	8.0	8.6	9.5	10.4	11.7
0.16	6.7	7.1	7.6	8.0	8.4	8.7	9.4	10.6	11.9
0.18	6.3	6.8	7.5	8.1	8.8	9.3	9.8	10.6	12.1
0.20	5.7	5.9	6.4	7.2	8.1	9.0	10.0	10.8	12.1
0.22	5.3	5.3	5.7	6.3	7.2	8.3	9.6	10.8	12.1

TABLE 11-16 Calculated Average *E*-Plane Beamwidth of a Log-Periodic Dipole Antenna for Length/Diameter = 70

	Scaling Constant, τ								
σ	0.80	0.82	0.84	0.86	0.88	0.90	0.92	0.94	0.96
0.06	60	59	86	78	61	69	66	62	58
0.07	76	61	57	73	69	67	64	61	56
0.08	83	76	61	63	71	61	64	60	55
0.09	75	83	72	60	62	69	62	58	54
0.10	57	76	81	72	63	62	62	58	53
0.12	66	61	60	63	69	65	59	57	51
0.14	73	69	67	65	63	63	61	54	50
0.16	64	65	64	63	62	63	61	54	49
0.18	69	66	66	64	60	58	56	55	48
0.20	78	80	80	76	71	64	57	53	48
0.22	81	81	86	84	79	71	62	55	48

TABLE 11-17 Calculated Average *H*-Plane Beamwidth of a Log-Periodic Dipole Antenna for Length/Diameter = 70

	Scaling Constant, τ								
σ	0.80	0.82	0.84	0.86	0.88	0.90	0.92	0.94	0.96
0.06	157	127	118	150	118	120	104	92	78
0.07	171	146	111	122	124	107	97	87	74
0.08	166	156	123	101	122	98	98	83	70
0.09	115	159	135	106	96	108	90	80	68
0.10	103	124	142	122	99	100	88	77	65
0.12	108	99	95	106	113	95	82	74	62
0.14	121	115	107	99	95	100	82	71	59
0.16	107	106	100	96	95	92	82	68	58
0.18	121	109	99	90	82	77	74	70	56
0.20	135	131	123	111	98	86	73	66	56
0.22		149	136	126	116	100	82	67	56

determine the number of elements required. The longest element length is given by

$$L_1 = K_1 \lambda_L \tag{11-27}$$

where λ_L is the longest operating wavelength and K_1 is the lower truncation constant.

We determine K_1 from the empirical equation [22]

$$K_1 = 1.01 - 0.519\tau \tag{11-28}$$

Equation (11-28) overestimates K_1 for $\tau > 0.95$, and the lower band edge will be extended slightly. We calculate the upper truncation constant from

$$K_2 = 7.08\tau^3 - 21.3\tau^2 + 21.98\tau - 7.30 + \sigma(21.82 - 66\tau + 62.12\tau^2 - 18.29\tau^3) \tag{11-29}$$

another empirical equation. The shortest element length is $L_U = K_2\lambda_U$, where λ_U is the shortest operating wavelength. We use the truncation constants and the frequency band edges to determine the number of dipoles in the antenna:

$$N = 1 + \frac{\log(K_2/K_1) + \log(f_L/f_U)}{\log \tau} \tag{11-30}$$

For a given frequency, $f_L = f_U = f$, and we compute the number of elements in the active region from Eq. (11-30):

$$N_a = 1 + \frac{\log(K_2/K_1)}{\log \tau} \tag{11-31}$$

Increasing the number of elements in the active region increases gain. We combine Eqs. (11-23) and (11-25) to determine the virtual apex distance:

$$R_n = \frac{2L_n\sigma}{1-\tau} \tag{11-32}$$

The axial length of the antenna is the difference between R_1 and R_N:

$$\text{length} = R_1 - R_N = R_1(1-\tau^{N-1}) = \frac{2L_1\sigma(1-\tau^{N-1})}{1-\tau} \tag{11-33}$$

We compute the dimensions of the antenna from the equations above by using an integer number of dipoles [Eq. (11-30)].

Example Design a log-periodic dipole antenna to operate from 100 to 1000 MHz.

Use $\tau = 0.9$ and $\sigma = 0.15$. We estimate the E- and H-plane average beamwidths from Tables 11-16 and 11-17.

$$E\text{-plane beamwidth} = 63^\circ \qquad H\text{-plane beamwidth} = 96^\circ$$

We use Eqs. (11-28) and (11-29) to compute the truncation constants: $K_1 = 0.54$ and $K_2 = 0.32$. We calculate the length L_1 by using K_1 and the lowest operating wavelength [Eq. (11-27)]: $L_1 = K_1\lambda_{100\,\text{MHz}} = 162\,\text{cm}$. We determine the number of elements from Eq. (11-30), $N = 28$, and substitute N into Eq. (11-33) to determine the total length, 457.7 cm. We rearrange Eq. (11-25) to calculate the first spacing, $d_1 = 2\sigma L_1 = 48.6\,\text{cm}$. We compute the virtual apex distance from Eq. (11-32):

$$R_1 = \frac{2L_1\sigma}{1-\tau} = 486\,\text{cm}$$

We use these dimensions and the scaling constant to iterate the rest of the antenna dimensions by using Eq. (11-22). For example,

$$L_2 = \tau L_1 = 145.8\,\text{cm} \qquad R_2 = \tau R_1 = 437.4\,\text{cm} \qquad d_2 = \tau d_1 = 43.74\,\text{cm}$$

We can estimate the gain from the length of the active region. We calculate the half apex angle from Eq. (11-26): 9.46°. The axial length of the active region

is $(K_1 - K_2)/\tan\alpha = 1.32\lambda$, and we use Eq. (10-12) for the directivity of a linear end-fire antenna:

$$\text{directivity} = \frac{4L}{\lambda} = 5.28 \ (7.2\,\text{dB})$$

The dipole pattern of the elements decreases the average radiation intensity and increases directivity by 1.4 dB, somewhat less than the 2.1 dB of the dipole because effective radiation length had already shaped the pattern. We read a gain of 8.6 dB from Table 11-15.

Table 11-15 has multiple points with similar gain. The length of the active region determines gain, but increasing the number of elements reduces the ripple in the frequency response. We can also reduce the ripple by increasing the element diameters or, equivalently, by using flat trapezoidal teeth for elements instead of thin dipoles. We substitute a dipole for a flat strip by using a diameter equal to half the strip width. Three antennas were designed to cover the frequency range 100 to 1000 MHz: (1) $\tau = 0.8$, $\sigma = 0.1$, and $L/d = 140$; (2) $\tau = 0.8$, $\sigma = 0.1$, and $L/d = 25$; (3) $\tau = 0.9$, $\sigma = 0.06$, and $L/d = 140$. The first two designs contain 16 elements with a boom length of 1.78 m, and the second one has 26 elements along a 1.96-m boom.

Figure 11-15 plots the frequency response of gain for the three designs. All three plots show narrow frequency ranges where the gain drops due to the combination of adverse coupling and feed network. This analysis ignores the currents induced on the feed lines, which produce additional dropout regions. When we use the lower truncation constant to design the longest element, the antenna has its full gain at the lower-frequency edge. The solid and long-dashed curves plot the responses of the antennas with $\tau = 0.8$ and $\sigma = 0.1$ and demonstrate a similar ripple period, whereas the design with more elements ($\tau = 0.9$ and $\sigma = 0.06$), plotted with short dashes, shows little ripple. The antenna with thin elements produces a design with more than 1 dB of gain ripple. The thicker elements also reduce the level of gain dropouts in the response.

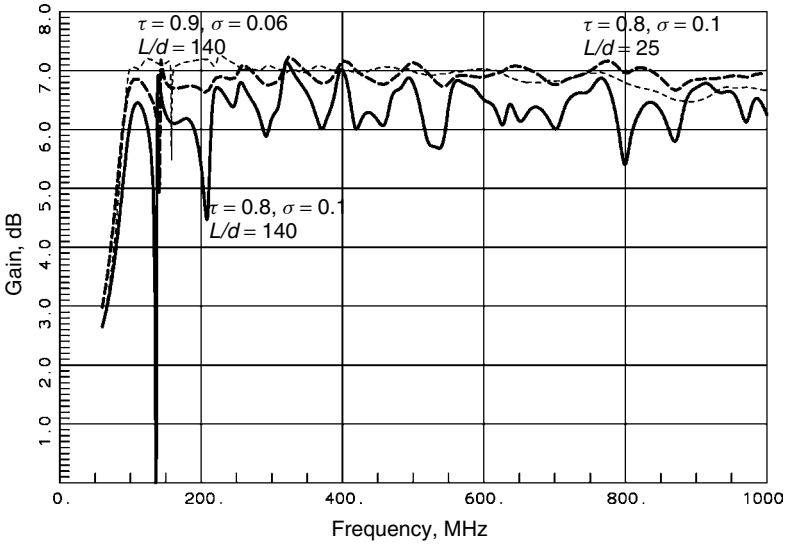

FIGURE 11-15 Frequency response of 16-element log-periodic dipole antennas designed for a 10 : 1 frequency range.

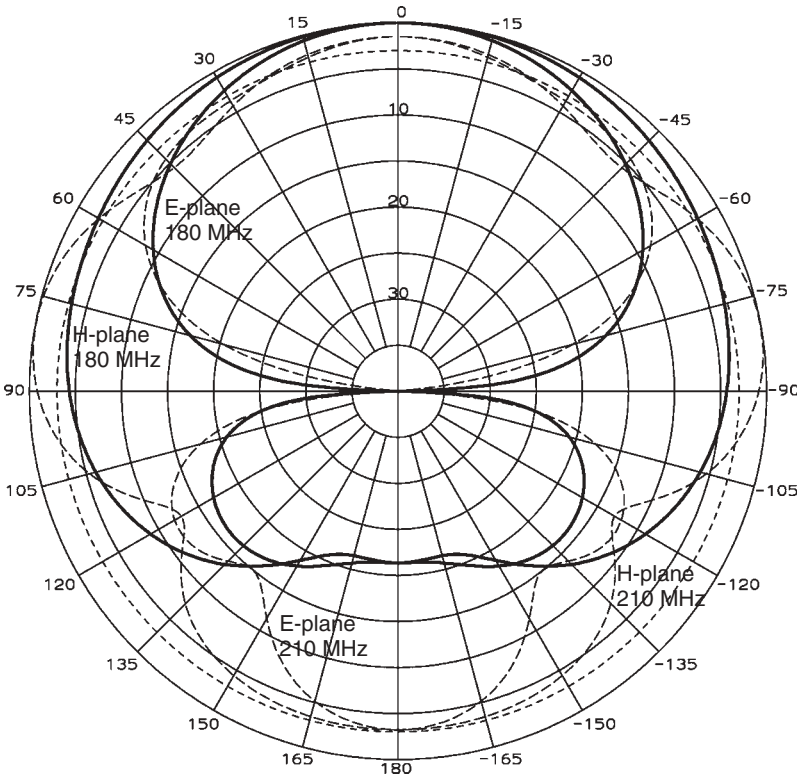

FIGURE 11-16 Patterns of a 16-element log-periodic dipole antenna with $\tau = 0.80$ and $\sigma = 0.1$.

Figure 11-16 gives the E- and H-plane patterns of case 1 at a normal frequency (180 MHz, solid) and at a frequency in the dropout region (210 MHz, dashed). The E-plane pattern contains a null at 90° due to the dipoles. The H-plane pattern shows how the pattern broadens and no longer has a traveling wave phasing along the elements in the active region to produce a significant front-to-back ratio. The pattern almost reduces to that of a single dipole. The front-to-back ratio is a more telling indicator than boresight gain of phasing problems in the log-periodic antenna. Antennas using thin dipoles and few elements in the active region have many regions with poor response. Increasing the diameter of the elements improves the F/B ratio. Increasing τ both improves F/B and increases the ripple rate.

11-12.1 Feeding a Log-Periodic Dipole Antenna

The antenna of Figure 11-14 must be fed from a balanced line; antennas designed for HF frequencies use that type of feed. If we can run a coax along the center of the antenna, we can use an infinite balun. We alternate the direction of the elements (Figure 11-17) on the outer shield of the coax feeder with a dummy coax to achieve the crisscross. The combination of the feed coax and dummy coax form a two-wire transmission line that feeds the elements. The truncation property of the antenna inhibits the flow of induced current on the feeder beyond the active region from reaching the input.

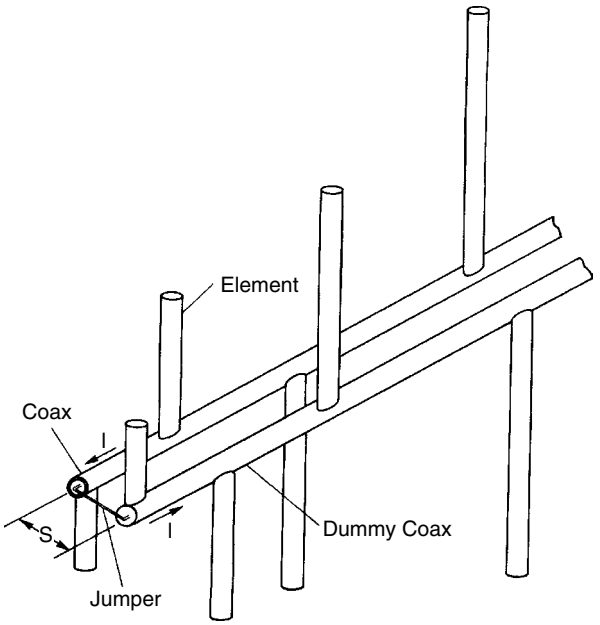

FIGURE 11-17 Log-periodic dipole antenna feed with an infinite balun.

We use a crisscross feed to increase the phase velocity on the feeder in the active region. If we used straight feeders between dipoles, the phase delay would equal that necessary for end fire in the direction of the feeder currents. This would produce a pattern in the direction of increasing structure and violate the truncation requirement. The extra 180° phase shift between elements produces a backfiring fast wave in the active region.

The region before the active region is a transmission line loaded with small open-circuited stubs (the dipoles). These capacitively load the line and reduce the effective characteristic impedance of the two-wire line. Each short dipole has capacitance

$$Z = -jZ_a \cot \frac{kL_i}{2} \tag{11-34}$$

where L_i is the total dipole length, k the wave number $(2\pi/\lambda)$, and Z_a the average characteristic impedance of the dipole:

$$Z_a = 120\left(\ln \frac{L_i}{2a} - 2.25\right) \tag{11-35}$$

for a dipole radius a. We use Eq. (11-35) with a constant length/diameter ratio in Eq. (11-34) to compute an effective added capacitance per unit length along the feeder due to the nonresonant dipoles. With a little manipulation we reduce this to an expression in terms of the log-periodic dipole antenna parameters. The effective feeder impedance R_0 is related to the unloaded two-wire impedance Z_0 by

$$R_0 = \frac{Z_0}{\sqrt{1 + (\sqrt{\tau} Z_0)/\sigma Z_a}} \tag{11-36}$$

If the length-to-diameter ratio of the dipoles remains constant, R_0 is constant along the antenna length. Even with a changing Z_0 or Z_a, the feeder acts as a tapered transmission-line transformer. We may expect impedance variations about the nominal value of Eq. (11-36) with a cycle of τ. The currents on the feeder radiate, but because they are close enough together and are nearly equal and opposite, they cancel in the far field. The feeder currents and the jumper at the feed limit the cross-polarization response to about 20 dB, which ripples with frequency changes.

The jumper between the center conductor of the coax feeder and the dummy coax line will squint the beam toward the dummy coax at high frequencies. We can represent the jumper as a series inductor in the transmission line, and construction difficulties with this jumper connection limit the high-frequency operation of log-periodic dipole antennas.

11-12.2 Phase Center

We expect the antenna phase center to be in the middle of the active region. If the antenna were made from many half-wavelength dipoles each resonant at a single frequency, we would look to the one $\lambda/2$ long at a given frequency to be the phase center. In the preceding example the active region dipoles ranged from 0.32λ to 0.54λ. We expect the phase center to be in front of the $\lambda/2$ element (or location along the triangle of the element ends of a possible element), since a great deal of the active region has elements of less than $\lambda/2$.

Table 11-18 lists the approximate E- and H-plane phase-center locations measured from the virtual apex relative to a $\lambda/2$ element. We may not have a $\lambda/2$ element at a given frequency; but given the envelope of elements defined by the apex angle, we compute the location of a possible element. Table 11-18 shows the astigmatism of the antenna with the H-plane phase center behind the E-plane phase center. The phase-center distance from the virtual apex increases linearly with λ.

Example Compute E- and H-plane phase centers of the antenna designed above for the range 100 to 1000 MHz ($\tau = 0.9$) at 600 MHz.

The half apex angle is 9.46°. The apex distance of the half-wavelength element is

$$R_g = \frac{\lambda}{4 \tan \alpha} = \frac{50}{4 \tan 9.46^\circ} = 75.02 \text{ cm}$$

TABLE 11-18 Log-Periodic Dipole Antenna Phase Center R_p Measured from the Virtual Apex Relative to the Location of a $\lambda/2$ Element $R_g = \lambda/(4 \tan \alpha)$

Scaling Constant, τ	R_p/R_g		Scaling Constant, τ	R_p/R_g	
	E-Plane	H-Plane		E-Plane	H-Plane
0.80	0.959	0.997	0.90	0.862	0.874
0.82	0.939	0.968	0.92	0.849	0.859
0.84	0.928	0.941	0.94	0.842	0.849
0.86	0.897	0.916	0.96	0.840	0.844
0.88	0.878	0.893			

Source: [22].

From Table 11-18 we read $R_p/R_g(E\text{-plane}) = 0.862$ and $R_p/R_g(H\text{-plane}) = 0.874$. The phase center distances from the virtual apex are

$$R_p(E - \text{plane}) = 64.67\,\text{cm} \quad R_p(H - \text{plane}) = 65.57\,\text{cm}$$

This astigmatism of 0.018λ produces an insignificant loss as a paraboloidal reflector feed (Figure 8-4).

11-12.3 Elevation Angle

The dipole elements must be connected alternately to the coax feeder and the dummy coax, but the feeder lines can diverge (Figure 11-18). We direct the feeder lines at angles $\pm\psi$ from the antenna axis. For the antenna to remain frequency independent, it is necessary for the projection of the two feeders to intersect at the virtual apex. Spacing the sides at angles $\pm\psi$ decreases the H-plane beamwidth since the aperture size increases in that plane. The elevation angle moves the antenna phase center toward the virtual apex and reduces movement with frequency changes. We must analyze the feeder line as a tapered transmission line. Moving the sides apart will increase the

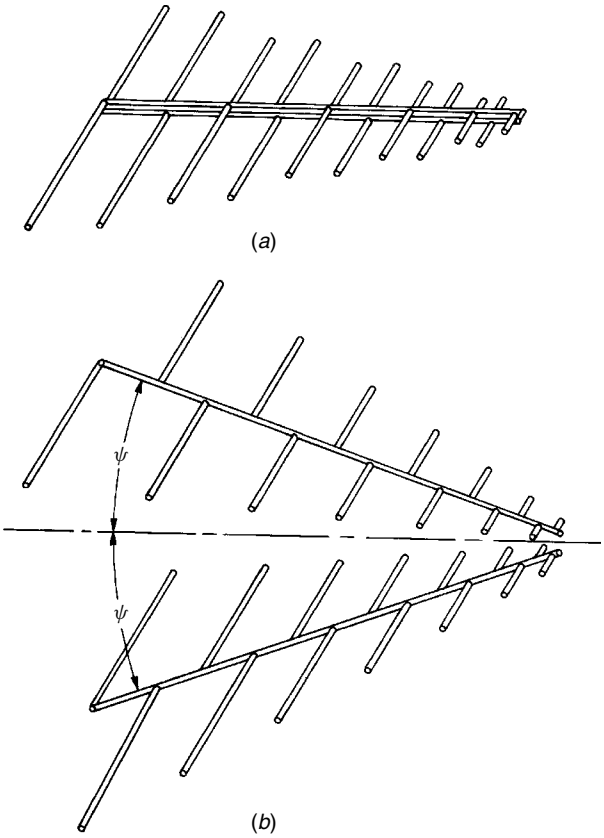

FIGURE 11-18 Log-periodic dipole antennas with the feeder diverged by elevation angle.

backlobe of the pattern because in the limit of $\psi = 90^\circ$, the front and back lobes are equal.

11-12.4 Arrays of Log-Periodic Dipole Antennas [24]

We can make broadband arrays with log-periodic antennas. Like the elevation angle of the single antenna, we have frequency-independent arrays only if the virtual apexes of all the elements of the array are coincident. The elements must also have the same τ and σ. Figure 11-19 shows E- and H-plane arrays. The relative phasing between elements can be changed in a frequency-independent manner. If an antenna is turned over, its far-field phase changes by 180°. In an array of two elements this will produce a null on the axis between them, the effect of placing a horizontally polarized antenna over a ground plane. On a particular antenna, if we multiply every element by the scaling constant, the far-field phase shifts by 180°. Multiplying every element by τ is equivalent to turning the antenna over (somewhere in the middle of the frequency band). Adding elements at the feed end does not change the location of the phase center. We can change the phase arbitrarily by multiplying the antenna dimensions by $\tau^{\gamma/180^\circ}$, where γ is the phase shift. Changing the phase by $\tau^{\gamma/180^\circ}$ has meaning only in an array.

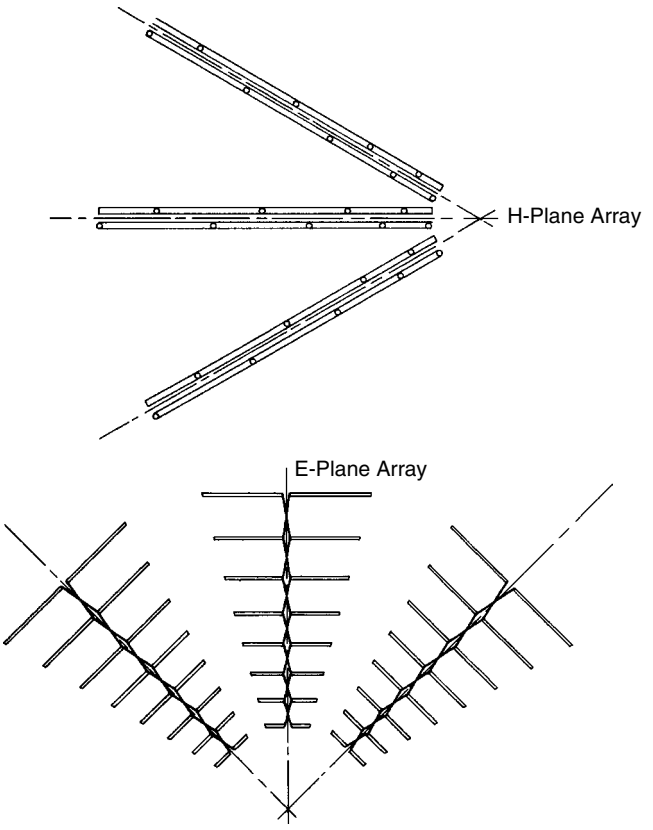

FIGURE 11-19 Arrays of log-periodic antennas.

We can build a frequency-independent circularly polarized antenna from two log-periodic antennas. We orient the two antennas at right angles with one of them scaled by $\tau^{1/2}$. When fed in phase, the pair combines 90° out of phase and radiates circular polarization. When we array log-periodic antennas, they may develop narrowband gain dropouts [25]. These dropouts occur in a sequence of frequencies with the scaling constant τ of the antenna. Antennas arrayed in either the E- or H-plane show these dropouts, as do antennas arrayed orthogonally. If we mismatch the scaling constants between the antennas in the array, each has dropouts scaled by its own scaling constant. Single antennas also can develop gain dropouts, although they seldom occur in a sequence of frequencies.

The phenomenon points to the importance of swept gain measurements because the location of the frequencies of dropouts remains somewhat unpredictable except for the sequence. Moment method models of the antenna will predict dropouts, but a large number of cases must be run to locate the frequencies. Unbalanced currents on the feeder lines interact with the elements to produce cross-polarization and large amounts of off-boresight radiation that lowers gain. These unwanted currents on the feeder are produced by either asymmetry in the antenna or interactions between antennas.

11-13 OTHER LOG-PERIODIC TYPES [26, 27]

Many different types of log-periodic antennas have been built. If we discover a structure that satisfies the self-scaling antenna requirements and has the desired polarization, we will have a new frequency-independent antenna. The first log-periodic antennas were teeth cut into the sides of bifin antennas. These radiated equally on both sides with polarization rotated parallel to the teeth instead of along the feed line. Isbell folded the sides at elevation angles to produce a unidirectional pattern. DuHamel and Ore [27] straighten the teeth to form the trapezoidal tooth antenna (Figure 11-20). We separate

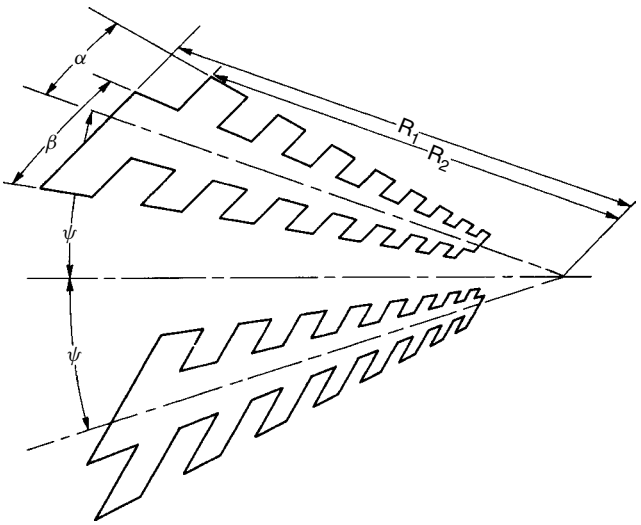

FIGURE 11-20 Trapezoidal tooth log-periodic antenna.

the sides by an angle 2ψ, and they project to the virtual apex. This is a good high-frequency antenna because it can be largely self-supporting. Figure 11-20 shows the teeth with the same width as the spacings. We can reduce the width of the teeth, but we continue to measure the distances R_n to the bottom of the teeth. As we continue to reduce the width of the teeth, the antenna transforms into a log-periodic dipole antenna.

When we remove material to form the teeth of a wire outline trapezoidal tooth antenna (Figure 11-21), it has only minor effects on the pattern. The shape of the teeth is not too important as long as the teeth scale with τ because the triangular tooth wire outline antenna (Figure 11-22) also works well. This tooth shape reduces some of the

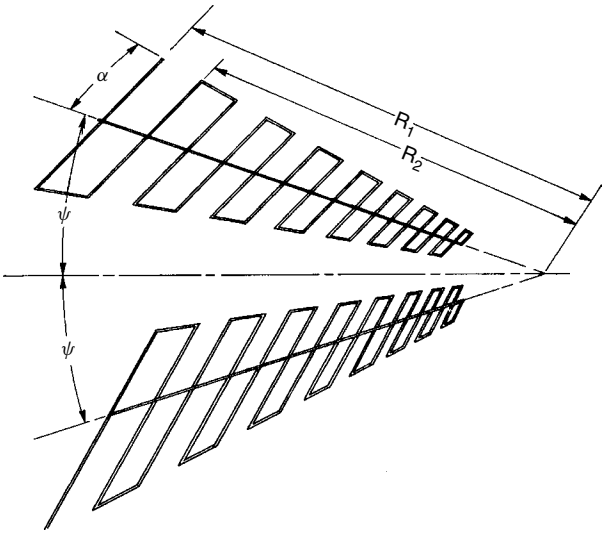

FIGURE 11-21 Trapezoidal tooth wire outline log-periodic antenna.

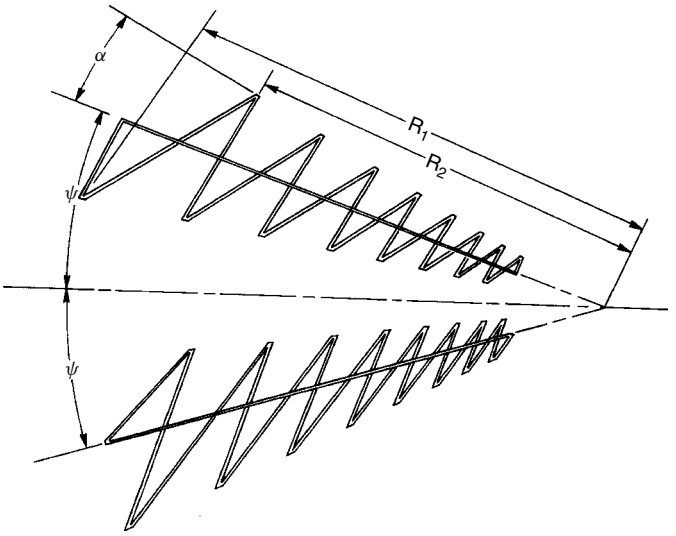

FIGURE 11-22 Triangular tooth wire outline log-periodic antenna.

TABLE 11-19 Trapezoidal Tooth Wire Outline Log-Periodic Antenna Designs

Scaling Constant, τ	Elevation Angle, ψ	Half Apex Angle, α	Beamwidth		Directivity (dB)	Sidelobes (dB)
			E-Plane	H-Plane		
0.63	15	30	85	153	5.0	12
0.63	15	37.5	74	155	5.6	12.4
0.71	15	30	70	118	7.0	17.7
0.71	15	37.5	66	126	7.0	17.0
0.63	22.5	30	86	112	6.3	8.6
0.63	22.5	37.5	72	125	6.6	11.4
0.71	22.5	30	71	95	7.9	14.0
0.71	22.5	37.5	67	106	7.6	14.9
0.77	22.5	30	67	85	8.6	15.8
0.84	22.5	22.5	66	66	9.8	12.3
0.84	22.5	30	64	79	9.1	15.8
0.63	30	30	87	87	7.4	7.0
0.63	30	37.5	73	103	7.4	8.6
0.71	30	30	71	77	8.8	9.9
0.71	30	37.5	68	93	8.1	12.8

Source: [27].

construction problems of the trapezoidal tooth design, especially at low frequencies. Because the wider teeth have greater coupling than dipoles, we can use smaller scaling constants τ and achieve good designs. Antennas have been built with $\tau = 0.63$, and the log-periodic dipole has a lower limit of about 0.80 for a good response. Table 11-19 lists the parameters of successful trapezoidal tooth wire outline antennas [27] in terms of log-periodic dipole parameters. Increasing the elevation angle decreases the H-plane beamwidth and raises the sidelobes. The H-plane beamwidth decreases as we increase the half apex angle, but the dipole-type pattern of the E-plane is its predominant factor. In the range of scaling constants given, the directivity increases with increasing scaling constant.

11-14 LOG-PERIODIC ANTENNA FEEDING PARABOLOIDAL REFLECTOR

The combination of a log periodic antenna feeding a paraboloidal reflector produces a wideband antenna with high gain. The significant problem is the movement of the phase center of the antenna over the frequency range, which causes phase error loss. For a given frequency range we locate the weighted-average phase center at the focus of the reflector. You determine the phase center by analysis or measurement at the lowest and highest frequencies of operation and calculate the best position to locate at the reflector focus:

$$PC_{\text{avg}} = \frac{PC_L F_L + PC_U F_U}{F_L + F_U} \tag{11-37}$$

This location of the phase center, PC_{avg}, produces the same loss at the lower frequency, F_L, and the upper frequency, F_U. You can extend Eq. (11-37) to include all frequencies for calculation of the average phase center as a weighted average. If you

build a log-periodic antenna using dipoles, having unequal beamwidths in the E- and H-planes generates cross-polarization in the diagonal plane when converted to dual-polarized Huygens sources. Each Huygens source excites uniformly polarized currents on the reflector. The nearly constant beamwidth of the antenna at all frequencies produces a constant sum of the spillover and taper loss over the frequency range of the feed operation.

Parameters for both broad- and narrowband designs were found to optimize the gain of the reflector using Carrell's analysis method [28]. Table 11-20 lists the design parameters of a wideband design given by the scaling constant τ and the half apex angle α. Antennas designed to the parameters of Table 11-20 to operate over a 10 : 1 frequency range were analyzed as feeds for a paraboloid reflector. We use Eq. (11-37) to locate the phase center so that we have the same phase error loss at the upper and lower frequencies. Table 11-21 lists the results.

TABLE 11-20 Parameters of Wide-Bandwidth Log-Periodic Dipole Feed for a Reflector

Reflector, f/D	Scaling Constant, τ	Half Apex Angle, α	Average Gain (dB)	Beamwidth	
				E-Plane	H-Plane
0.25	0.855	41.7	6.1	61.3	143.3
0.30	0.867	40	6.0	73.0	141.4
0.35	0.869	37.5	6.1	72.2	139.4
0.40	0.900	32	6.5	69.3	126.0
0.45	0.914	27	6.8	67.0	124.1
0.50	0.923	22	7.3	66.6	112.2
0.55	0.928	20	7.4	66.9	112.4
0.60	0.934	17.5	7.8	65.5	105.6
0.65	0.940	16	8.0	64.2	101.0
0.70	0.944	13.5	8.4	62.7	94.2
0.75	0.947	12	8.8	61.6	90.0

TABLE 11-21 Reflector Illumination Losses of Log-Periodic Dipole Antennas Designed to Operate over a 10 : 1 Frequency Range

Reflector, f/D	Number of Elements	Maximum PEL (dB)	Average ATL (dB)	Average SPL (dB)	Cross-Polarization Loss	Total (dB)		
						Minimum	Maximum	Average
0.25	19	0.60	1.52	0.46	0.40	2.32	3.37	2.64
0.30	21	0.44	0.95	0.73	0.36	1.93	2.94	2.20
0.35	23	0.53	0.97	0.71	0.35	1.97	2.95	2.23
0.40	26	0.38	0.44	1.22	0.32	2.05	2.60	2.21
0.45	30	0.40	0.36	1.52	0.28	2.10	2.70	2.30
0.50	33	0.44	0.26	1.63	0.23	2.04	2.80	2.28
0.55	36	0.38	0.20	1.90	0.21	2.19	3.08	2.44
0.60	40	0.38	0.16	2.07	0.17	2.30	3.10	2.53
0.65	43	0.34	0.12	2.33	0.15	2.48	3.30	2.73
0.70	47	0.36	0.11	2.40	0.11	2.50	3.40	2.74
0.75	50	0.36	0.09	2.55	0.09	2.61	3.50	2.85

Repeating the analysis of the antennas in Table 11-21 over a 20 : 1 frequency range for f/D between 0.30 and 0.50 increased the maximum loss by only 0.1 dB. The wideband antennas use short lengths to limit the phase-center movement as the operating frequency changes and radiate wide H-plane beamwidths from their short active region. The ideal feed for a reflector has nearly equal beamwidths to reduce spillover and reduce cross-polarization in the diagonal planes. Table 11-22 gives a second set of designs that produce optimum illumination from the log-periodic dipole antenna for a narrow band of frequencies. If we consider an additional 0.5 dB loss, similar to the 2 : 1 VSWR, the bandwidth of these antennas is approximately 70%, or equivalently, a 2 : 1 frequency range. Of course, the antenna needs to be designed with sufficient elements to cover the frequency range.

We reduce the number of elements required by using a trapezoidal tooth design (Figure 11-20). These designs work best with a reflector f/D between 0.40 and 0.55. We separate the sides by an angle 2ψ to decrease the H-plane beamwidth. Table 11-23 lists the results from a method of moments analysis for varying ψ on an antenna designed to operate over a 10 : 1 frequency range (16 elements) with $\tau = 0.80$, $\sigma = 0.125$ ($\alpha = 21.8^\circ$), and tooth width/element spacing $= \frac{1}{3}$. The MOM analysis includes the currents flowing on the feeder lines that radiate increasing cross-polarization as the sides separate. This design peaks at $f/D = 0.48$. Table 11-24 shows that the illumination losses change very slowly for different f/D and it is difficult to say that the feed peaks for a particular f/D.

A trapezoidal tooth log-periodic antenna was built and tested as a feed for a reflector. Table 11-25 lists the average and maximum sum of the illumination losses calculated

TABLE 11-22 Optimum Narrowband Log-Periodic Dipole Antennas Reflector Feeds

f/D	Scaling Constant, τ	α	Gain (dB)	Beamwidth (deg)		ATL (dB)	SPL (dB)	Cross-Polarization Loss	Minimum Total (dB)
				E-Plane	H-Plane				
0.30	0.920	18.5	7.7	66.6	108.1	1.35	0.27	0.18	1.79
0.35	0.928	15	8.1	64.1	99.8	1.00	0.33	0.13	1.46
0.40	0.940	12	8.7	61.8	90.1	0.78	0.39	0.10	1.23
0.45	0.944	10	9.1	60.3	85.5	0.61	0.47	0.08	1.10
0.50	0.947	8.2	9.6	58.4	79.6	0.50	0.52	0.06	1.02
0.55	0.952	7	10	56.5	74.3	0.42	0.58	0.04	0.99
0.60	0.952	5.3	10.7	53.8	68.0	0.34	0.54	0.03	0.96

TABLE 11-23 Trapezoidal Tooth Log-Periodic Antenna Feed for a Reflector with $f/D = 0.48$, 10 : 1 Frequency Range (16 Elements) with $\tau = 0.80$, $\sigma = 0.125$ ($\alpha = 21.8^\circ$)

ψ	Beamwidth (deg)		Maximum PEL (dB)	Average ATL (dB)	Average SPL (dB)	Average XOL (dB)	F/B (dB)	Total (dB)	
	10-dB E-Plane	10-dB H-Plane						Average	Maximum
5	108.1	180.4	0.54	0.44	1.13	0.23	20	1.98	2.51
10	108.0	158.1	0.53	0.45	0.93	0.26	15	1.82	2.37
15	110.2	143.3	0.57	0.42	0.83	0.38	13	1.87	2.52
20	113.5	124.7	0.49	0.52	0.84	0.60	12	2.15	2.80

TABLE 11-24 Illumination Loss Variation for Trapezoidal Tooth Log-Periodic Antenna Reflector Feed Over a 10 : 1 Frequency Range (16 Elements) with $\tau = 0.80$, $\sigma = 0.125$ ($\alpha = 21.8^\circ$), and $\psi = 15^\circ$

	f/D							
Loss (dB)	0.40	0.42	0.44	0.46	0.48	0.50	0.52	0.54
Average	1.94	1.88	1.86	1.85	1.87	1.91	1.95	2.01
Maximum	2.80	2.68	2.60	2.54	2.52	2.52	2.53	2.55
Minimum	1.58	1.54	1.53	1.55	1.58	1.67	1.67	1.73

TABLE 11-25 Measured Illumination Losses for Trapezoidal Tooth Log-Periodic Antenna Reflector Feed Over a 6 : 1 Frequency Range with $\tau = 0.80$, $\sigma = 0.1$ ($\alpha = 26.6^\circ$), and $\psi = 6^\circ$

	f/D							
Loss (dB)	0.40	0.42	0.44	0.46	0.48	0.50	0.52	0.54
Average	1.78	1.69	1.64	1.63	1.64	1.68	1.74	1.82
Maximum	2.73	2.53	2.38	2.28	2.24	2.40	2.47	2.56

At $f/D = 0.46$:

Beamwidth (deg)		Maximum	Average	Average	Average	Average	Maximum
10-dB E-Plane	10-dB H-Plane	PEL (dB)	ATL (dB)	SPL (dB)	XOL (dB)	Total (dB)	Total (dB)
107.6	147.0	0.58	0.49	0.63	0.28	1.63	2.28

from measurements over a 6 : 1 frequency range. An infinite balun feed was made by attaching the feeding coax to the central plate of one side and connecting the coax center conductor to a coax outer shield attached to the second arm. Small movements between the two sides rapidly alter the input impedance, and a few experiments involving changing their spacing produce an acceptable return loss. Table 11-25 shows results similar to Table 11-24 in that the antenna has a broad optimum affected very little by the reflector parameters. This antenna has an improved performance relative to the preceding design (Tables 11-23 and 11-24) because it operates over a 6 : 1 bandwidth instead of 10 : 1.

Increasing α to 30° ($\sigma = 0.0866$) makes the antenna shorter, and its performance peaks for $f/D = 0.42$ for the same 10 : 1 frequency range and $\tau = 0.8$. Table 11-26 lists the parameters of this design. Although this design peaks for $f/D = 0.42$, the losses increase only slowly when we change f/D, similar to the design in Table 11-24. For higher f/D we need narrower beamwidths to reduce spillover, which requires a design with a longer active region. The longer antenna will have a greater phase-center movement over the frequency range. A design that peaks at about $f/D = 0.54$ uses $\tau = 0.84$ and $\sigma = 0.125$ ($\alpha = 17.7^\circ$). Table 11-27 lists the results for this antenna.

A paper by DuHamel and Ore [29] reports the results of measurements of trapezoidal tooth log-periodic feeds for reflectors. These antennas use small scaling constants τ,

TABLE 11-26 Trapezoidal Tooth Log-Periodic Antenna Feed for a Reflector with $f/D = 0.42$

	Beamwidth (deg)		Maximum	Average	Average	Average		Total (dB)	
	10-dB	10-dB	PEL	ATL	SPL	XOL	F/B		
ψ	E-Plane	H-Plane	(dB)	(dB)	(dB)	(dB)	(dB)	Average	Maximum
5	116.1	203.8	0.38	0.44	1.09	0.29	23	1.96	2.16
10	114.4	186.5	0.38	0.49	0.90	0.28	18	1.80	2.04
15	114.9	179.2	0.36	0.52	0.82	0.31	17	1.78	2.01
20	116.1	166.0	0.35	0.56	0.79	0.41	13	1.90	2.15

TABLE 11-27 Trapezoidal Tooth Log-Periodic Antenna Feed for a Reflector with $f/D = 0.54$, 10 : 1 Frequency Range (16 Elements) with $\tau = 0.84$, $\sigma = 0.125$ ($\alpha = 17.7^\circ$)

	Beamwidth (deg)		Maximum	Average	Average	Average		Total (dB)	
	10-dB	10-dB	PEL	ATL	SPL	XOL	F/B		
ψ	E-Plane	H-Plane	(dB)	(dB)	(dB)	(dB)	(dB)	Average	Maximum
5	107.2	158.5	0.56	0.30	1.27	0.21	20	1.97	2.45
10	107.5	139.5	0.54	0.32	1.04	0.33	16	1.87	2.57
15	110.6	118.4	0.53	0.36	0.95	0.60	14	2.09	3.00
20	114.4	97.3	0.49	0.47	1.04	0.95	8	2.64	3.82

TABLE 11-28 Trapezoidal Tooth Log-Periodic Antenna Feed for a Reflector with $f/D = 0.46$

	Beamwidth (deg)		Maximum	Average	Average	Average		Total (dB)	
	10-dB	10-dB	PEL	ATL	SPL	XOL	F/B		
ψ	E-Plane	H-Plane	(dB)	(dB)	(dB)	(dB)	(dB)	Average	Maximum
10	102.5	181.4	0.32	0.49	1.24	0.76	13	2.62	3.64
22.5	105.4	154.7	0.36	0.56	1.17	1.14	8	3.01	4.55

Source: [29].

wide half apex angles α, and widely separated sides ψ to reduce the reflector feed phase error loss due to axial defocusing. The paper reports results over a large range of parameters. Two of the better ones were analyzed as a feed for a reflector with $f/D = 0.46$. These antennas have a scaling constant $\tau = 0.707$ and a half apex angle $\alpha = 30^\circ$ ($\sigma = 0.127$). Table 11-28 lists analysis results of two designs; both produce high cross-polarization loss due to feed line radiation and unequal E- and H-plane beamwidths.

11-15 V LOG-PERIODIC ARRAY [30]

A V log-periodic antenna sweeps the dipole elements of the log-periodic antenna shown in Figure 11-14 forward to form a series of V dipoles. This antenna can be operated

over a large frequency range such that the dipoles operate in higher-order modes. The dipoles operate in $\lambda/2$ mode at the lowest frequencies and are then scattered among a series of transition frequency bands of poor performance. The antenna operates again in $3\lambda/2$, $5\lambda/2$, $7\lambda/2$, and so on, modes of the dipoles. Dipoles, resonant in the higher-order modes, radiate multiple lobe patterns. In a log-periodic antenna these lobes produce high sidelobes. To reduce these sidelobes the elements are swept forward so that the pattern nulls are aligned with the poles that reduce them. The antenna does not need the

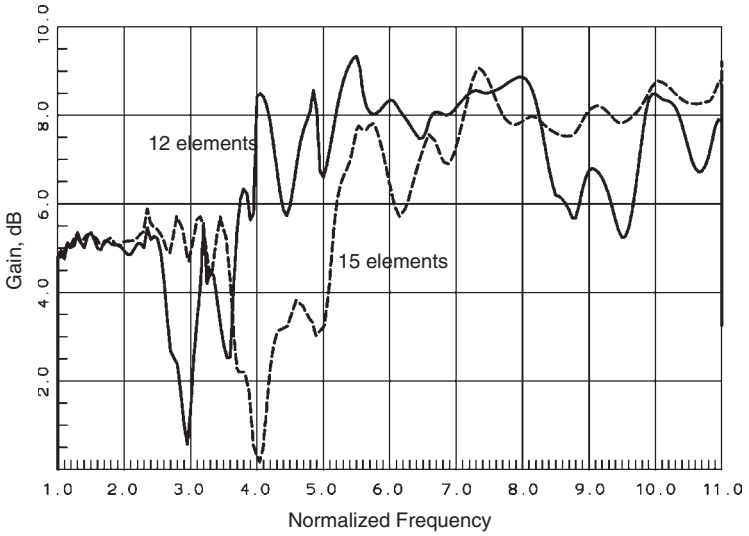

FIGURE 11-23 V-dipole log-periodic antenna gain for $\tau = 0.9$, $\sigma = 0.05$, $\psi = 45°$.

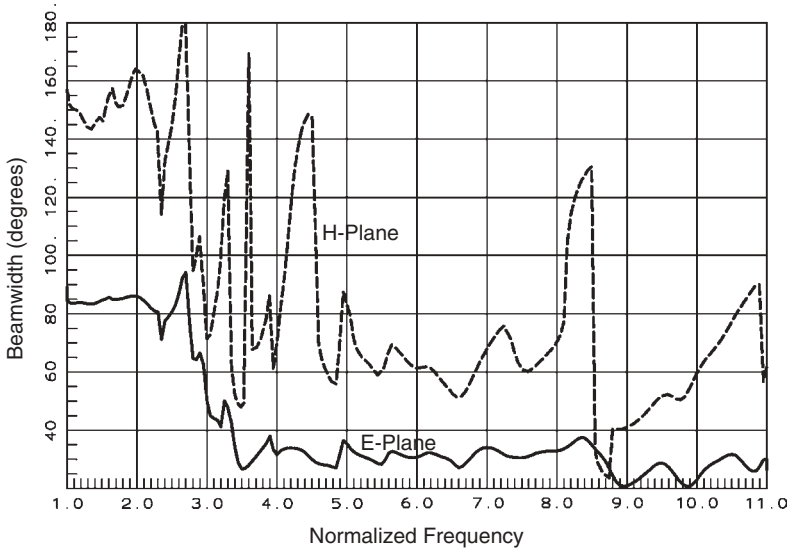

FIGURE 11-24 V-dipole log-periodic antenna beamwidth for $\tau = 0.9$, $\sigma = 0.05$, $\psi = 45°$: 12 elements (solid curve); 15 elements (dashed curve).

small dipoles required for high frequencies in normally designed log-periodic dipole antennas, which eases construction problems.

Designs use scaling constants $\tau \geq 0.9$ and small spacing constants $\sigma \leq 0.05$. Two antennas were designed with 12 and 15 elements using these factors and analyzed. The 12-element antenna requires a dipole length ratio of 3.2 across the elements and has a length of 0.37λ at the lowest frequency; the 15-element antenna dipole length ratio is 4.37, with a boom length 0.42λ at the lowest frequency. Figure 11-23 gives the gain versus normalized frequency found by reducing directivity by the reflected power loss due to impedance mismatch. The poor impedance match reduces gain in the band 2.7 to 3.7 for the 12-element antenna and 3.7 to 5.2 for the 15-element antenna. The return loss is better than -6 dB (3 : 1 VSWR) over the remaining frequency range. Figure 11-24 shows that the E-plane beamwidth decreases drastically when the antenna operates in the higher-order dipole modes. The H-plane pattern exhibits considerable variation and at some frequency ratios has large sidelobes that reduce gain. We cannot use the beamwidths to estimate directivity, but must integrate the entire pattern. The 12-element antenna has its shortest elements 2λ long at the highest frequency.

11-16 CAVITY-BACKED PLANAR LOG-PERIODIC ANTENNAS

We use some of the original planar log-periodic antennas that have wide beamwidth patterns on both sides and eliminate one side by placing it on a cavity in the same manner as a spiral. By using elements morphed into arcs, we interleave two or more antennas to build an antenna to radiate dual linear polarization, or we can combine the two linear polarizations with a hybrid power divider (0° and 90° phases) to obtain RHC and LHC polarization. Similar to a spiral, we can design antennas with multiple spiral modes by interleaving more than two antennas in a single aperture.

Figure 11-25 shows a layout of the interlog antenna [31] that contains two planar log-periodic antennas interleaved. We design such antennas using normal log-periodic antenna design procedures and roll the poles into arcs. We feed the antenna from the center and mount it over an absorber-loaded cavity. The antenna can radiate either dual linear or dual circular polarizations, depending on the feed network. The typical

FIGURE 11-25 Interlog antenna.

predicted pattern of the antenna when fed for RHC polarization is similar to a spiral. The log-periodic nature of the antenna produces a lower amplitude pattern at $\theta = 90^\circ$ than a spiral. Although the antenna has four arms, we cannot form a mode 2 spiral beam because generating circular polarization consumes a degree of freedom. The antenna shown in Figure 11-25 has a 1.54λ circumference at the lowest frequency. Interleaving causes problems because the coupling produces pattern distortion periodic with frequency. The cross-polarization for an antenna fed RHC increases and beamwidth broadens over narrow frequency ranges. We reduce this effect by decreasing the interleaving, but antenna size grows.

The second example of a planar log-periodic antenna over a cavity is a sinuous antenna [32,33]. The triangular tooth antenna has been morphed into arcs using a sinuous curve to reduce reflections from the corners (Figure 11-26). We use the same sinuous curve to define both edges of each arm by rotating it about the center axis. Similar to the interlog antenna, we can feed the four-arm antenna for dual linear or dual circular polarizations. The sinuous antenna radiates a pattern similar to a spiral. To design these antennas we make the sweep of the curved triangles $\lambda/4$, although it is one-half the dipole of a log-periodic antenna. Given the angle of the triangle sweep of the sinuous antenna, $\alpha + \delta$ (rad), we compute its length from the center distance r:

$$\text{length} = r(\alpha + \delta) = \frac{K_1 \lambda}{2} \tag{11-38}$$

We determine the factor K_1 from Eq. (11-28) for the lower truncation constant given τ, the scaling constant. A recommended value for $\alpha + \delta$ is 67.5° for a four-arm antenna that produces a self-complementary structure. We compute the circumference from the lowest frequency and K_1:

$$\text{circumference} = \frac{\pi K_1 \lambda_L}{\alpha + \delta} \text{ (rad)} = \frac{180^\circ K_1 \lambda_L}{\alpha + \delta} \approx \frac{\pi \lambda_L}{2(\alpha + \delta)} \tag{11-39}$$

For $\tau = 0.8$, Eq. (11-28) gives $K_1 = 0.595$. When we use $\alpha + \delta = 67.5^\circ$ for the four-arm antenna and insert these values in Eq. (11-40), we compute circumference $= 1.58\lambda$, a value similar to that for the interlog antenna.

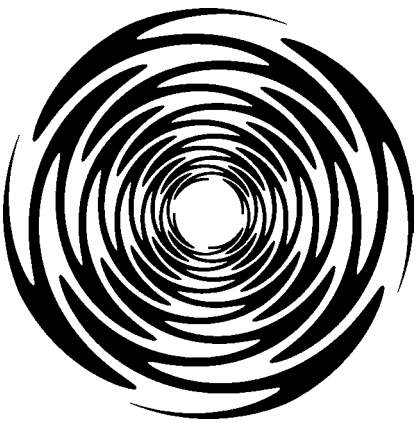

FIGURE 11-26 Sinuous antenna.

When we use a sinuous antenna for dual linear polarization, we discover that the polarization direction oscillates about $\pm 3^\circ$ when we vary frequency. The two directions track each other for both pairs of a four-arm structure, and cross-polarization is reduced when we feed it to radiate circular polarization.

REFERENCES

1. V. H. Rumsey, Frequency independent antennas, *1957 IRE National Convention Record*, pt. 1, pp. 114–118.
2. V. H. Rumsey, *Frequency Independent Antennas*, Academic Press, New York, 1966.
3. R. G. Corzine and J. A. Mosko, *Four-Arm Spiral Antennas*, Artech House, Boston, 1990.
4. E. M. Turner, Spiral slot antenna, *Technical Note WCLR-55-8*, Wright Air Development Center, Dayton, OH, June 1955.
5. J. A. Kaiser, The Archimedean two-wire spiral antenna, *IRE Transactions on Antennas and Propagation*, vol. AP-8, May 1960, pp. 312–323.
6. G. A. Deschamps, Impedance properties of complementary multi-terminal planar structures, *IRE Transactions on Antennas and Propagation*, vol. AP-7, special supplement, December 1959, pp. S371–S378.
7. J. A. Huffman and T. Cencich, Modal impedances of planar, non-complementary, N-fold symmetric antenna structures, *IEEE Antennas and Propagation Magazine*, vol. 47, no. 1, February 2005.
8. K. C. Gupta, R. Garg, and R. Chadha, *Computer Aided Design of Microwave Circuits*, Artech House, Boston, 1981.
9. J. Svacina, A simple quasi-static determination of basic parameters of multilayer microstrip and coplanar waveguide, *IEEE Microwave and Guided Wave Letters*, vol. 2, no. 10, October 1992, pp. 385–387.
10. J. D. Dyson, The equiangular spiral antenna, *IRE Transactions on Antennas and Propagation*, vol. AP-7, no. 2, April 1959, pp. 181–186.
11. R. Bawer and J. J. Wolfe, A printed circuit balun for use with spiral antennas, *IRE Transactions on Microwave Theory and Techniques*, vol. MTT-8, May 1960, pp. 319–325.
12. T. A. Milligan, Parameters of a multiple-arm spiral antenna from single-arm measurements, *IEEE Antennas and Propagation Magazine*, vol. 40, no. 6, December 1998, pp. 65–69.
13. V. A. Monaco and P. Tiberio, Automatic scattering matrix computation of microwave circuits, *Alta Frequenza*, vol. 39, February 1970, pp. 59–64.
14. P. G. Ingerson, Modulated arm width spiral antenna, U.S. patent 3,681,772, August 1, 1972.
15. J. D. Dyson, The unidirectional equiangular spiral antenna, *IRE Transactions on Antennas and Propagation*, vol. AP-7, no. 5, October 1959, pp. 329–334.
16. J. D. Dyson, The characteristics and design of the conical log-spiral antenna, *IEEE Transactions on Antennas and Propagation*, vol. AP-13, no. 4, July 1965, pp. 488–498.
17. C. S. Liang and Y. T. Lo, A multiple-field study for the multiarm log-spiral antennas, *IEEE Transactions on Antennas and Propagation*, vol. AP-16, no. 6, November 1968, pp. 656–664.
18. G. A. Deschamps and J. D. Dyson, The logarithmic spiral in a single-aperture multi-mode antenna system, *IEEE Transactions on Antennas and Propagation*, vol. AP-19, no. 1, January 1971, pp. 90–96.
19. A. E. Atia and K. K. Mei, Analysis of multiple-arm conical log-spiral antennas, *IEEE Transactions on Antennas and Propagation*, vol. AP-19, no. 3, May 1971, pp. 320–331.

20. D. E. Isbell, Log periodic dipole arrays, *IRE Transactions on Antennas and Propagation*, vol. AP-8, no. 3, May 1960, pp. 260–267.

21. R. L. Carrel, The design of log-periodic dipole antennas, *1961 IRE National Convention Record*, pt. 1, pp. 61–75.

22. C. E. Smith, *Log Periodic Design Handbook*, Smith Electronics, Cleveland, OH, 1966.

23. R. L. Carrel, Analysis and design of the log-periodic dipole antenna, *Antenna Laboratory Technical Report 52*, University of Illinois, Urbana, IL, October 1961.

24. R. H. DuHamel and D. G. Berry, Logarithmically periodic antenna arrays, *1958 IRE National Convention Record*, pt. 1, pp. 161–174.

25. K. G. Balmain and J. N. Nkeng, Asymmetry phenomenon of log-periodic dipole antennas, *IEEE Transactions on Antennas and Propagation*, vol. AP-24, no. 4, July 1976, pp. 402–410.

26. R. H. DuHamel and D. E. Isbell, Broadband logarithmically periodic antenna structures, *1957 IRE National Convention Record*, pt. 1, pp. 119–128.

27. R. H. DuHamel and F. R. Ore, Logarithmically periodic antenna designs, *1958 IRE National Convention Record*, pt. 1, pp. 139–151.

28. W. A. Imbriale, Optimum designs of broad and narrow band parabolic reflector antennas fed with log-periodic dipole arrays, *IEEE AP-S Symposium Digest*, vol. 12, June 1974, pp. 262–265.

29. R. H. DuHamel and F. R. Ore, Log periodic feeds for lens and reflectors, *1959 IRE National Convention Record*, March 1959, pp. 128–137.

30. P. E. Mayes and R. L. Carrel, Logarithmically periodic resonant-V arrays, *IRE WESCON Convention Record*, pt. 1, 1961.

31. D. A. Hofer, O. B. Kesler, and L. L. Loyet, A compact multi-polarized broadband antenna, *IEEE Antennas and Propagation 1990 Symposium Digest*, pp. 522–525.

32. R. H. DuHamel, Dual polarized sinuous antenna, U.S. patent 4,658,262, April 1987.

33. R. H. DuHamel and J. P. Scherer, Frequency-independent antennas, Chapter 14 in R. C. Johnson, ed., *Antenna Handbook*, 3rd ed., McGraw-Hill, New York, 1993.